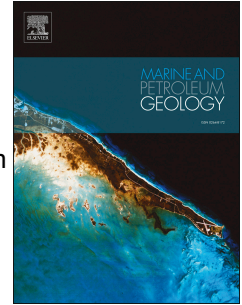


Accepted Manuscript

Impacts of small-scale faults on continental to coastal plain deposition: Evidence from the Realgrunnen Subgroup in the Goliat field, southwest Barents Sea, Norway

Mark Joseph Mulrooney, Bjarte Rismyhr, Honore Dzekamelive Yenwongfai, Johan Leutscher, Snorre Olaussen, Alvar Braathen



PII: S0264-8172(18)30197-1

DOI: [10.1016/j.marpetgeo.2018.04.023](https://doi.org/10.1016/j.marpetgeo.2018.04.023)

Reference: JMPG 3330

To appear in: *Marine and Petroleum Geology*

Received Date: 14 July 2017

Revised Date: 2 January 2018

Accepted Date: 30 April 2018

Please cite this article as: Mulrooney, M.J., Rismyhr, B., Yenwongfai, H.D., Leutscher, J., Olaussen, S., Braathen, A., Impacts of small-scale faults on continental to coastal plain deposition: Evidence from the Realgrunnen Subgroup in the Goliat field, southwest Barents Sea, Norway, *Marine and Petroleum Geology* (2018), doi: [10.1016/j.marpetgeo.2018.04.023](https://doi.org/10.1016/j.marpetgeo.2018.04.023).

This is a PDF file of an unedited manuscript that has been accepted for publication. As a service to our customers we are providing this early version of the manuscript. The manuscript will undergo copyediting, typesetting, and review of the resulting proof before it is published in its final form. Please note that during the production process errors may be discovered which could affect the content, and all legal disclaimers that apply to the journal pertain.

Impacts of small-scale faults on continental to coastal plain deposition: Evidence from the Realgrunnen Subgroup in the Goliat field, Southwest Barents Sea, Norway.

Mark Joseph Mulrooney^{1, 3}; Bjarte Rismyhr^{1, 2}; Honore Dzekamelive Yenwongfai³; Johan Leutscher⁴; Snorre Olaussen¹; Alvar Braathen^{1,3}

1. Department of Arctic Geology, University Centre in Svalbard (UNIS), PO Box 156, 9171 Longyearbyen, Svalbard, Norway
2. Department of Earth Science, University of Bergen, PO Box 7803, N-5020 Bergen, Norway
3. Department of Geosciences, University of Oslo (UiO), PO Box 1047 Blindern 0316 OSLO, Norway
4. Eni Norge AS, PO Box 101 Forus, 4064 Stavanger, Norway

Corresponding author: mark.mulrooney@geo.uio.no

ABSTRACT

In this study we synthesise sedimentological, fault, and Amplitude Versus Angle (AVA) analysis and propose that the Fruholmen and Tubåen formations (Realgrunnen Subgroup) are syn-kinematic deposits that record a previously undocumented early phase of Mesozoic rifting on the Troms-Finmark fault Complex and within the Hammerfest Basin. The Realgrunnen Subgroup hosts one of two Triassic reservoirs currently being produced in the Goliat field. Here, the subgroup sits unconformably on top of the Storfjorden Subgroup (Carnian Snadd Formation). Away from the Goliat field, which is characterised by a periclinal anticline, the Realgrunnen Subgroup also comprises the Lower–Middle Jurassic Nordmela and Stø formations.

Sedimentological analysis of six exploration wells reveals that the Fruholmen Formation was deposited in a prodelta to delta plain environment where tide-influenced and fluvial-dominated distributary channels are represented by clay/siltstones and very fine grained sandstones. The overlying Tubåen Formation is characterised by medium to very coarse-grained deposits (locally conglomeratic) and represents a widespread braid plain with localised alluvial fans.

Displacement profiles of faults and along-fault thickness variations demonstrate that an immature fault system was active during deposition of the Realgrunnen Subgroup. A series of

unconnected fault segments hosted isolated sub-basins and erosional catchment areas in their hanging and foot walls, respectively. An AVA attribute map generated from a 10 ms interval of the uppermost part of the subgroup reveals the geometries of gross sand prone depositional bodies, i.e., individual and amalgamated channels, (some of which show meandering geometries), ox-bow lakes and alluvial fans. Sand bodies frequently show elongate geometries parallel to faults indicative of syn-depositional fault-related subsidence.

Driving mechanisms responsible for the Norian to Rhaetian event may relate to contemporaneous rejuvenation of the Fennoscandian hinterland, development of the Novaya Zemlya fold-and-thrust belt and/or the early Cimmerian tectonic phase in northern Europe.

1. INTRODUCTON

The surface expression of faulting, i.e., tectonic geomorphology, in a rift basin has a strong local effect on sedimentation. Tectonically induced slopes, i.e., tilting, becomes a primary control on drainage and erosional patterns, flood distribution, as well as the location, geometry, and style of deposition. The sedimentary response (Fig. 1) to these vertical movements varies with regard to the stage of rift development, depositional setting, i.e., continental vs. marine, and climatic conditions (Alexander & Leeder, 1987; Leeder & Gawthorpe, 1987; Gawthorpe & Colella, 1990; Prosser, 1993; Gupta et al., 1999; Gawthorpe and Leeder, 2000).

Extensional faults form geometrically coherent systems of discontinuous segments which grow incrementally over time amounting displacement during earth quake rupture events. These fault segments show systematic displacement to length scaling. As faults grow, relay zones form between neighbouring segments that allow transfer of displacement (i.e., soft linkage). Subsequent growth results in relay zone breach and the establishment of through-going faults. (Watterson, 1986; Walsh & Watterson, 1988; Marrett & Allmendinger, 1991; Peacock, 1991; Peacock and Sanderson, 1991; Walsh and Watterson, 1991; Cowie & Scholz, 1992; Dawers et al., 1993; Trudgill & Cartwright, 1994; Cartwright et al., 1995, 1996; Dawers & Anders, 1995; Childs et al., 1995, 1996; Willemse et al., 1996; Meyer et al., 2002; Wilkins and Gross, 2002; Childs et al., 2002; Soliva & Benedicto, 2004; Walsh et al., 2003; Kim et al., 2005; Bull et al., 2006; Kristensen et., al 2008; Nicol et al., 2010; Childs et al., 2016).

Undulations in the geometry of a mature, through-going fault can reflect its linkage history (e.g., Peacock and Sanderson, 1991; Mansfield & Cartwright, 1996, 2001; Walsh et al., 2003; Lohr et al., 2008). For example, displacement minima and kinks in fault strike/dip occur at sites of segment linkage. Moreover, the rock volume surrounding faults is geometrically and coherently linked to fault movement. As displacement accrues, the footwall and hanging wall experience uplift and

subsidence, respectively (Barr, 1987; Wernicke & Axen, 1988; Yielding, 1991; Long & Imber, 2010) which can be described in terms of longitudinal (sub-parallel to fault) and transverse (orientated at high angles to faults) folding as depicted in Fig. 1.

Transverse hanging wall synclines form individual isolated basins associated within hanging walls of individual fault segments. These basins coalesce over time in response to fault linkage. Contemporary to increase in hanging wall accommodation space, the corresponding upwards movement in the footwall prompts erosion and the establishment of semi-circular drainage catchments characterised by erosional linear channels fed by larger dendritic channel systems (Leeder, 1991; Leeder & Jackson, 1993; Eliet & Gawthorpe, 1995; Densmore et al., 2003, 2004; Foster et al., 2010; Elliott et al., 2011). Relay zones and erosional fault scarps act as loci for drainage entering rift basins. Typical early stage rift deposits include continental alluvial fans (Hooke, 1967; Nemeč & Postma, 1993; Blair & McPherson, 1994; Harvey et al., 2005; Longhitano et al., 2015) or fan deltas (Holmes, 1965, Rust, 1979; Friedman & Sanders, 1978; Ethridge & Wescott, 1984; Nemeč & Steel, 1988; Postma, 1990; Longhitano, 2008; Longhitano et al., 2015). Both deposits consist of coarse siliciclastics that are usually immature to submature, both texturally and mineralogically.

Fault related subsidence and uplift (along with climate change and eustatic sea-level), can modify the dynamic equilibrium profile of a depositional system tract (Mackin, 1948; Schumm, 1993; Blum & Törnqvist, 2000; Holbrook et al., 2006). In fluvial and deltaic environments, axial through-flowing river channels and delta lobes tend to migrate or avulse towards the axis of maximum subsidence, i.e., parallel to the structural strike (Bridge and Leeder, 1979; Miall et al., 1981). Preferential flooding of the down-tilted side of the floodplain also occurs. Channels become more confined due to tilting, leading to a dominance of stacked channel geometries. (Gupta et al., 1999; Young et al., 2002; Garcia-Garcia et al., 2006). Individually, tilting can cause sand bodies to become abnormally wide and asymmetric (Alexander & Leeder, 1987).

In this contribution, we use sedimentological, fault, and Amplitude Versus Angle (AVA) analysis from the Goliat field to consider the depositional environments of late Norian to Rhaetian deposits of the Realgrunnen Subgroup and to establish the time from which Mesozoic rifting initiated in the Hammerfest Basin.

2. GEOLOGICAL BACKGROUND

The Hammerfest Basin (Rønnevik & Jacobsen, 1984; Berglund et al., 1986; Gabrielsen et al., 1990; Knutsen & Vorren, 1991; Ostanin et al., 2012; Indrevær et al., 2017; Mulrooney et al., 2017) is a relatively shallow Mesozoic basin with a depth to basement of approximately 5 to 6 km compared to the deeper Tromsø and Nordkapp basins where this depth can exceed 10 km (Øvrebø & Talleraas, 1977; Henriksen et al., 2011). The basin (Fig. 2B) ranges between 50–75km wide, is elongate in the

ENE-WSW direction and is situated on the south-western flank of the Barents Shelf (Rønnevik, 1981; Rønnevik et al., 1982; Faleide et al., 1984, 1993; Rønnevik and Jacobsen, 1984; Dengo and Røssland, 1992; Gudlaugsson et al., 1998; Stemmerik, 2000).

The Hammerfest Basin is separated from the Finnmark Platform to the southeast by the Troms-Finnmark Fault Complex (TFFC). Separation from the Tromsø Basin in the west is defined by the approximately N–S striking Ringvassøy-Loppa Fault Complex (RLFC) whereas the eastern border has the nature of a flexure against the Bjarmeland Platform (Gabrielsen et al., 1990). The basin is asymmetric with the deepest part in the north adjacent to the Asterias Fault Complex which delineates the basin from the Loppa High. The basin can be subdivided into east and west sub-basins (Ziegler et al., 1986) which may correlate with the offshore prolongation of the Trollfjord-Komagelva Fault Zone (Gabrielsen & Færseth, 1989; Gabrielsen et al., 1990; Roberts and Lippard, 2005; Gernigon et al., 2014). At the margins, the basin exhibits deep-seated, high-angle faults in addition to shallower normal faults that detach within the Permo-Carboniferous strata (Gabrielsen and Færseth, 1989; Mulrooney et al., 2017).

Internally, the fault populations strike parallel to the basin delineating faults i.e., the north–south striking RLFC, the E–W to ESE–WNW striking Hammerfest Basin Regional fault system and the variably orientated segments of the TFFC (Gabrielsen, 1984; Mulrooney et al., 2017). The TFFC parallels the shoreline of the Troms and Finnmark counties and delineates the Finnmark Platform in the south from basins to the north including the Harstad, Tromsø and Hammerfest basins (Fig. 2B). The complex, or fault system, consists of several hard-linked segments which exhibit orientations of NNE-SSW to NE-SW in the south, ENE-WSW (informally, the Alke-Goliat segment) in the centre (Fig. 3), and NNE-SSW (informally, the Goliat-Tornerose segment) towards the northeast (Fig. 3).

The central part of the Hammerfest Basin is characterised by a gentle domal structure, which strikes parallel to the basin axis and is underpinned by the Hammerfest Basin Regional fault system, genesis of the feature has been tentatively linked to the Cimmerian tectonic phase (Øvrebø & Talleraas, 1977). The structural grain of the Hammerfest basin, especially the basin–platform delineating TFFC (Øvrebø & Talleraas, 1977; Rønnevik et al., 1982; Gabrielsen, 1984; Gabrielsen et al., 2011; Gabrielsen & Færseth, 1988, 1989; Indrevær et al., 2013) is suggested to reflect a Caledonian lineament. Separation of the Hammerfest Basin from the Finnmark Platform is envisaged to have taken place in the Late Carboniferous.

The Triassic in the Barents Shelf is described generally as a period of tectonic quiescence (Riis et al., 2008; Worsley et al., 2008; Glørstad-Clark et al., 2011; Høy & Lundschieen, 2011) with ongoing regional subsidence, however, local zones of fault activity persisted, e.g., the southern Loppa High Fault System (Gabrielsen, 1984; Indræver et al., 2016), the Hoop Graben (Mahajan et al.,

2014), eastern Svalbard (Anell et al., 2013; Osmundsen et al., 2014), and segments of the TFFC (this contribution). During this time, the Hammerfest Basin likely formed part of a larger epeirogenic depositional regime, although Berglund et al. (1986) identify it as a separate depocentre from the Early Triassic onwards. The latest Permian to Middle Triassic is dominated by deltaic sequences which prograded across the entire Barents Shelf (Glørstad-Clark et al., 2010, 2011; Anell et al., 2014). The Ingøydjupet Subgroup was primarily sourced from the uplifted Uralides, but the Baltic Shield also contributed and is likely a more prominent source for the southern Hammerfest Basin including the Goliat field (Riis et al., 2008; Mørk, 2009). The Middle to Late Triassic (comprising the Ingøydjupet and Storfjorden Subgroups) saw the shelf edge prograde north-westwards as far as Svalbard (Anell et al., 2014). The Realgrunnen Subgroup is most completely developed in the south-western Barents Sea where it consists of mature sandstones deposited in coastal plain and deltaic to shallow marine environments (Olaussen et al., 1984; Berglund et al., 1986; Worsley et al., 2008; Henriksen et al., 2011). Dominant lithologies comprise sandstones and shales with subordinate conglomerates, carbonates and coals. Deposition ranged from the Late Triassic to Middle Jurassic. The Realgrunnen and Ingøydjupet subgroups host the target reservoirs in the Goliat field. Only the lower part of the Realgrunnen Subgroup is preserved in the Goliat field, the Fruholmen Formation and lower part of the Tubåen Formation. Together these formations define a 67–118 m thick unit and form the upper Goliat reservoir. Palaeodrainage during the Rhaetian to Hettangian, i.e., during deposition of the Tubåen Formation (Fig. 4) is envisaged to have flown from east to west within the central axis of the Hammerfest Basin, while in the Goliat field, a more northwest to west-northwest palaeo-direction is evident (Fig. 4).

The main phase of Mesozoic rifting took place in the Middle Jurassic to Early Cretaceous (Gabrielsen et al., 1990; Faleide et al., 2008). Primary fault complexes such as the TFFC developed large accommodation zones adjacent to active segments. A large domal structure formed contemporaneously to this fault's activity in the hanging wall of the TFFC which Gabrielsen et al. (1990) describe as a roll-over structure. Mulrooney et al. (2017), however, credit this structure to differential subsidence on two vertical segments of the TFFC. The central dome in the Hammerfest Basin is also believed to have developed at this time (Gabrielsen et al., 1990). The precise timing of the initiation of this stage of rifting is ambiguous. In the south-western Barents Shelf, the top Realgrunnen Subgroup is defined by a Middle Jurassic regional unconformity (Henriksen et al., 2011).

3. STRUCTURAL ARCHITECTURE OF THE GOLIAT FIELD

The Goliat field consists of Middle to Late Triassic reservoirs which exploit an elongate anticline (the Goliat anticline) in the hanging wall of the TFFC (Mulrooney et al., 2017). The field is

situated within a complex zone of deformation associated with a major bend in the TFFC. Key structural elements affecting the field are summarised here and within Fig. 3. The Goliat anticline is affected by three primary fault populations, two of which exhibit trends parallel to TFFC segments, i.e., the Goliat–Tørnerose (GT) segment (030–210°) and the Alke–Goliat (AG) segment (085–265°). A third 102–282° trending fault population represents the Hammerfest Regional fault system (Gabrielsen et al., 1984). A local NW–SE trending fault population, the Goliat Central (GC), is seen to only affect the Goliat anticline. Subsidiary faults to the west of the Goliat exhibit curvilinear traces where they show an Alke–Goliat trend to the south and a Goliat–Tørnerose trend to the north (Mulrooney et al., 2017). The Goliat field is dominated by 5 large segments of the Troms-Finnmark Fault Complex, the GT1 fault (the largest fault in the area), the AG1, AG2, AG3 and AG4. The HR1 fault is not considered a TFFC segment, and instead is suggested to represent an offshore extension of the Trollfjord-Komagelva Fault Zone (Gabrielsen & Færseth, 1989; Gabrielsen et al., 1990; Roberts and Lippard, 2005; Gernigon et al., 2014).

The Goliat anticline is underlain by a 10 km wide, basement fault block (Mulrooney et al., 2017) which is bound by two vertical segments of the TFFC. Mulrooney et al. (2017) suggested the western limb of the Goliat anticline formed by differential subsidence across the TFFC segments. The eastern limb, in contrast has been credited to hanging wall roll-over related to ramp-flat-ramp to listric geometries on the TFFC.

The Goliat crest forms a culmination in the Goliat anticline. The structure has a complex history and formed as a transverse fold at the site of linkage between two former segments of the GT1 fault. Moreover, the transverse fold is superimposed on the Goliat anticline. The Goliat crest forms a displacement minimum on the GT1 fault and divided depocentres during the initial stages of Mesozoic rifting on the GT1. Former segmentation of the GT1 is also evident from sharp jogs in the fault trace and dip. Mulrooney et al. (2017) suggest the fault existed as at least three segments prior to amalgamation during the Late Triassic to Early Jurassic. The AG1 exists as a series of left-stepping partially breached en-echelon segments at the level of the Realgrunnen Subgroup. Down-section, the structure becomes through-going.

Mesozoic syn-kinematic geometries in the hanging wall of the GT1 fault are consistent with deposition during up-section propagation of a blind fault, over which, a monocline was established and later breached. Rifting took place in the Palaeozoic (Carboniferous to Permian?), and in the Mesozoic, possibly as early as the Late Triassic, with a major event in the Late Jurassic to Early Cretaceous. Minor reactivations continued into the Late Cretaceous, and possibly the Early Cenozoic.

A phase of Barremian inversion created local compression structures above blind extensional faults as well as deeper seated buttressing against large faults (Indrevær et al., 2017;

Mulrooney et al., 2017). A non-tectonic polygonal fault system affects the Late Cretaceous to Early Cenozoic succession and is comparable to the Campanian succession of the Western Hammerfest Basin (Mulrooney et al., 2017).

4. DATA AND METHODS

The dataset for the sedimentological study comprises wireline logs and 235 m of slabbed core from six exploration wells (Table 1) in the Goliat field (PL229 and PL229B). The seismic study was conducted using the EN0901 multi-azimuth (MAZ) three-dimensional seismic survey. Both core and seismic data were provided by Eni Norge. The seismic survey is a pre-stack, depth migrated 3D dataset and covers an area of approximately 207 km² and provides imagery down to 4000 m depth. The EN0901 MAZ consisted of a single source with a dense streamer configuration. The seismic data were acquired using a shot point interval of 12.5 m and a streamer length of 4000m. Survey azimuths of 7°, 67° and 127° were chosen to best illuminate the multiple fault trends.

Observations and measurements from the cores included lithology, colour, thicknesses, grain size, sorting, sedimentary structures, bed boundaries, fossils and bioturbation. The degree of bioturbation follows the Bioturbation Index (BI) of Taylor & Goldring (1993). The observed sedimentary features were used to group the deposits into facies reflecting discrete depositional elements or environments. Composite wireline log suites, which included gamma ray (GR), neutron-porosity (NP) and bulk density (BD) logs, were used for a more simplistic recognition and interpretation of lithologies, boundaries and relating non-cored intervals to the sedimentary facies framework. A well-to-well correlation was subsequently performed using facies architecture and stacking patterns, and guided by in-house (Eni Norge) palynological data.

The seismic interpretation workflow focused on identifying depositional geometries of the Realgrunnen Subgroup and high resolution mapping of faults. The workflow was conducted using the Petrel E&P Software Platform. The well ties for the Late Triassic and Jurassic successions are shown in Fig. 5. A more in depth seismic work flow is described in Mulrooney et al. (2017). Fault polygons and seismic horizons were imported into Badley's T7 software where hanging and footwall cut-offs were computed for four master faults, AG1, AG2, AG3 and HR1 and seven subsidiary faults AG5, AG6, AG7, GT2, GT3, GT4 and GT5, locations of which are shown in Fig. 3. Displacement analysis was conducted using a sampling interval of 100 m and produced a series of Alan diagrams. In addition, footwall and hanging wall packages were projected onto the fault plane in order to determine near-fault thickness variations. Hanging wall thickness maxima and foot wall minima were correlated in order to identify isolated depocentres and sites of erosion.

AVA (Amplitude Versus Angle) attribute analysis was conducted on a time-depth cube of the EN0901 multi-azimuth (MAZ) survey. Analysis was conducted over a 10 ms window below the top

Realgrunnen Subgroup using HampsonRussel AVO analysis & Modelling software. The method was used to highlight the gross sand prone areas and depositional geometries of the Realgrunnen Subgroup. Insights from the sedimentological, fault and seismic attribute analyses were synthesized and used to develop palaeogeographic reconstructions for the upper Fruholmen Formation and the Tubåen Formation in the Goliat area.

5. SEDIMENTOLOGICAL FACIES ANALYSIS

Eight sedimentary facies were defined from the analysis of core and wireline log data. One of the facies (facies 3) was subdivided into subfacies based on subtle sedimentological differences observed in core, which could otherwise not be distinguished from wireline log signatures alone. Facies characteristics are summarised in Table 2 and key sedimentary structures and interpretations for each facies are given below. A log key is displayed in Fig. 6.

5.1 FACIES 1 – DISTAL ALLUVIAL FAN

Description. Facies 1 comprises a 7.5 m thick sandstone body in 7122/7-3 (Fig. 7) which consists of poorly sorted, coarse- to very coarse-grained sandstones with rare, scattered gravel and pebbles. The sandstones are pale yellow in colour with occasional cm-thick reddish-stained horizons, and show no clear internal grain size trends. Extraformational subangular fine gravel (maximum particle size; MPS 5 mm) and subangular to subrounded mudstone and siltstone pebbles (MPS 5 cm, long axis, Fig. 7A) are randomly dispersed throughout facies 1 and show no preferred orientation. Boundaries between individual beds are generally indistinct with no apparent erosional relief, although crudely stratified cm- to dm-thick sandstone beds are locally observed. The sandstones are mostly massive and structureless (Fig. 7A) except for rare dm-thick horizons with diffuse low-angle cross-stratification (Fig. 7B). No bioturbation is present. The lower boundary of facies 1 is not observed in core, but wireline log signatures suggest it abruptly overlies deposits of facies 4. Facies 1 is replaced upward by facies 2. Facies 1 is characterised by a box-shaped GR log response and a large negative separation between NP and BD curves.

Interpretation. The massive, structureless appearance of the sandstones, the coarse sediment fraction and texturally immature character of the deposits of facies 1 is interpreted to be the result of rapid deposition in areas proximal to an active sediment source. The scarcity of cross-stratification and scour surfaces is taken to indicate a non-channelized depositional setting, and the massive sandstones of facies 1 are suggested to represent the deposits of unconfined cohesionless debris flows (e.g. Nemeč and Steel, 1984; Postma, 1986) in a distal alluvial fan setting. The reddish colouration is taken to indicate well-drained oxidising conditions which further point towards a fully terrestrial environment. The absence of bioturbation supports this interpretation. Rare diffusely cross-stratified sandstone horizons likely reflect periodic tractional transport within shallow

channels. The scarcity of pebbles is taken to indicate a distal position on the alluvial fan, although clast composition and size are largely controlled by the lithology in the drainage basin (e.g., Blair, 1999).

5.2 FACIES 2 – FLUVIAL BRAIDPLAIN

Description. Facies 2 consists of 0.1 to 1.2 m thick beds of poorly to moderately sorted, fine- to very coarse- (locally gravelly) sandstones organised in 1-5 m thick sharp-based fining-upward (FU) units (Fig. 7). Together, the FU units stack to form composite sandstone bodies up to 10 m thick. Gravel, mudstone rip-up clasts and, more rarely, coal fragments are concentrated at the base of FU units, on internal scour (bedding) surfaces and on cross-strata foresets (Fig. 7C,F,I). The sandstones are trough and planar cross-stratified (Fig. 7C,D,G-I), locally passing up into current ripple- and plane-parallel lamination (Fig. 7H). No bioturbation is observed. At the top of facies 2, a 40-50 cm thick mottled and multi-coloured (yellow, orange and red) carbonate cemented sandstone bed with possible root casts is present (Fig. 7E). Facies 2 sharply overlies deposits of facies 3a and facies 4. The lower boundary in well 7122/7-3 is less distinct and may be gradational with facies 1. Facies 2 is characterised by cylindrical GR log responses and negative separation between NP and BD curves.

Interpretation. Facies 2 is interpreted as fluvial braidplain deposits. This is based on the sharp bases, the vertical stacking of FU units, and the dominance of cross-stratification which suggest sustained flow in a channelised setting (Collinson, 1996). The abundance of internal scour surfaces and the lack of intervening fine-grained floodplain deposits is probably related to juxtaposition of channel units within mobile channel belts. The presence of mudstone rip-up clasts suggests that fine-grained material was deposited between individual channels, but were not preserved in situ. The mottled, carbonate cemented bed developed at the top of Facies 2 is tentatively interpreted as a palaeosol level formed under a period of prolonged subaerial exposure and oxidising conditions.

5.3 FACIES 3 – FLUVIAL CHANNEL

Facies 3 is characterised by cylindrical to bell-shaped GR curves and either no or a large negative separation between NP and BD curves. Based on subtle sedimentological differences observed in core, facies 3 has been subdivided into two subfacies (3a and 3b).

5.4 SUBFACIES 3A – FLUVIAL CHANNEL

Description. This facies consists of 0.1 to 1.0 m thick beds of very fine- to very coarse-grained moderately to well-sorted sandstones forming 3.0 to 10.0 m thick sharp-based single or stacked units with upward fining grain-size motifs. Structureless, trough- and planar cross-stratified fine- to very coarse-grained sandstones (Fig. 8A, F) dominate in the lower part of facies 3a, passing upward

into very fine- to fine-grained sandstones with current-ripple and plane-parallel lamination (Fig. 8D). Rootlets may be present at the top. Plant material is abundant throughout and rip-up mudstone clasts occur as lags on basal and internal scour surfaces. Up to 1 m thick heterolithic intervals consisting of thin-bedded mudstones and very fine-grained sandstones with synaeresis cracks, flaser-, wavy- and current ripple-lamination are locally present at the top of individual units.

Interpretation. Based on the sharp bases, the FU trend, the dominance of tractional and current generated sedimentary structures, and the abundance of plant material, facies 3a is interpreted as fluvial channel deposits. Thicker successions of facies 3a (e.g. 1154-1137 m MD 7122/7-6) are interpreted to reflect accumulation within trunk rivers (e.g. Olariu & Bhattacharya, 2006), whereas FU units only a few meters thick may represent deposits of relatively shallow distributary channels mostly unaffected by basinal processes in the upper delta plain. The vertical arrangement of sedimentary structures and the FU trend is taken to record progressive waning of energy during channel filling (Bridge, 2006). Heterolithic intervals developed at the top of some FU units are interpreted as passive channel fills (i.e., abandonment fills) accumulated from overbank sedimentation following abrupt abandonment of channels through upstream channel plugging or avulsion.

5.5 SUBFACIES 3B – TIDE-INFLUENCED DISTRIBUTARY CHANNELS

Description. Facies 3b consists of 0.1 to 2.0 m thick beds of very fine- to coarse-grained sandstones forming 1-9 m thick sand bodies with FU trends and sharp bases. Heterolithic intervals up to 1 m thick with alternating thin-bedded wavy to lenticular laminated silty mudstones and very fine-grained sandstones may be present within and at the top of individual units. The sandstones are moderately to well sorted and characterised by trough and planar cross-stratification locally with tangential set bases (Fig. 8A-C,E), which passes upward into current ripple- (2D and 3D ripples), plane-parallel- and flaser lamination. Mm- to cm-thick single and paired drapes of mud and organic debris are abundant throughout facies 3b and accentuate cross-strata and ripple foresets (Fig. 8A-C,E). Mudstone rip-up clasts and coal fragments are present at bed bases and internal scour surfaces, and plant material is scattered throughout. Rootlets may be present at the top of individual FU units. The degree of bioturbation is low (BI 0-2), consisting of undifferentiated simple vertical and horizontal burrows (Fig. 8B,E) mainly confined to beds and laminae composed of silty mudstone and very fine-grained sandstone.

Interpretation. Facies 3b is interpreted as tide-influenced distributary channel deposits. This is based on the sharp and erosive bases, the FU grain size trends, the dominance of tractional and current generated sedimentary structures, which as for facies 3a point toward deposition in a fluvial channelised setting. The abundance of single and paired mud drapes is interpreted to reflect

variations in flow stages as a result of tidal influence (e.g., Gastaldo et al., 1995; Visser, 1980; Martinius & Gowland, 2011; Longhitano et al., 2012; Longhitano et al., 2017; Mellere et al., 2017), and suggests the distributary channels were located within the reach of tidal incursions of sea water. This is supported by the higher degree of bioturbation in facies 3b compared to facies 3a, which may suggest some influence of marine waters.

5.6 FACIES 4 – FLOODPLAIN/DELTA PLAIN

Description. This subfacies comprises 1.0 to 24.0 m thick heterolithic successions of mudstone, siltstone, thin coals and fine- to very fine-grained sandstone (Fig. 9). Mudstones and siltstones are massive or finely laminated, and brownish, grey and dark grey in colour. Sandstones range in thickness from a few millimetres to 2.0 m (commonly <0.5 m thick), have sharp or gradational bed boundaries and may fine or coarsen slightly upward. Current ripple lamination (2D and 3D-ripples) dominates in the sandstones (Fig. 9B, C) with climbing current ripple-lamination, plane-parallel lamination and small-scale planar cross-stratification occurring less frequently. Plant material, coal fragments and rootlets (Fig. 9D,H) are ubiquitous. Bioturbation intensity is variable (BI 0-4) and characterised by relatively simple undifferentiated vertical and horizontal burrows, occasionally sand-filled. Escape traces and soft-sediment deformation structures are locally observed (Fig. 9B). Facies 4 is characterised by relatively high GR values but with highly irregular and serrated wireline log patterns.

Interpretation. Based on the heterolithic, mudstone-dominated character of facies 4, the abundance of rootlets and plant material, and the vertical association with facies 3, this facies is interpreted as floodplain/delta plain deposits. The mudstones and siltstones are related to deposition from suspension on the floodplain and within shallow delta plain lakes or bays during floods. The sandstones were probably deposited as a variety of crevasse channel, crevasse splay, levee and overbank lobe deposits sourced from adjacent rivers. Rooted horizons reflect soil formation, and the presence of thin carbonaceous mudstones and coals reflect periodic accumulation of peats, suggesting water-saturated and stagnant conditions. Small-scale upward coarsening-units with rooted tops are interpreted as bay-fills and were formed by progradation of crevasse splays or minor mouth bars (Elliot, 1974).

5.7 FACIES 5 – DELTA FRONT

Description. Facies 5 includes up to 5-6 m thick sandstone dominated heterolithic successions composed of 1-4 m thick single or stacked upward-coarsening units (Fig. 10) which locally alternate vertically with deposits of facies 6. Facies 5 has transitional lower boundaries towards deposits of facies 6, whereas upper boundaries may be both conformable (towards facies 4

and 6; Fig. 10) and erosional (towards facies 3). Internal bed boundaries are commonly conformable. The upward coarsening units have heterolithic bases composed of interbedded mudstone, siltstone and very fine-grained sandstone, and grade upward into very fine- to fine-grained sandstone characterised by plane-parallel and low-angle cross-lamination, planar cross-stratification, current ripples (locally climbing), wave ripples and combined flow ripples. Rootlets and root casts are common towards the top of individual upward coarsening units (Fig. 10D, E), whereas synaeresis cracks and dish structures are locally observed. Bioturbation is generally moderate but highly variable (BI 1-5), and includes *Lockeia*, *Planolites*, *Teichichnus*, *Diplocraterion*, *Palaeophycus*, *Rosselia*, *Skolithos* and rare fugichnia. In wireline logs facies 5 is characterised by funnel-shaped and slightly irregular GR log responses and weak positive or no separation between the NP and BD curves.

Interpretation. Facies 5 is interpreted to comprise distributary mouth bars deposited in a delta front setting. This is based on the presence of sandstone-dominated upward-coarsening units with rooted tops, and the mix of sedimentary structures, which reflect deposition in relatively high energy environments under the action of both unidirectional and oscillatory traction currents. Common wave and combined flow ripples reflect modification of the mouth bar deposits by fairweather waves. Relatively high sedimentation rates and rapid deposition can be inferred based on the presence of climbing current ripples, fugichnia and dish structures, whereas synaeresis cracks and the variable bioturbation intensity may reflect fluctuating salinity levels. The ichnological assemblage, which is attributed to a distal expression of the *Skolithos* ichnofacies (MacEachern et al., 2007) is consistent with a relatively high energy marginal marine depositional setting. The limited thickness of individual upward-coarsening units is taken to suggest relatively shallow water depths, and the vertical alternation with prodelta deposits (facies 6) is interpreted to reflect autocyclic delta lobe switching due to upstream avulsion of the feeding distributaries (e.g., Bhattacharya, 2006).

5.8 FACIES 6 – PRODELTA

Description. This facies is present in the lower 23-33 m of the Fruholmen Formation (Fig. 10A-D,G), and comprises dark grey laminated mudstone with sporadically distributed carbonaceous detritus, and more heterolithic intervals consisting of mm- to cm-thick, locally siderite-cemented, interbedded grey mudstone, siltstone and mm to cm-thick sandstone (Fig. 10B, C, G). Normal graded beds up to a few centimetres in thickness are relatively common in the heterolithic intervals (Fig. 10A-C, G), and fine upward from very fine-grained sandstone at the base to siltstone and mudstone. Synaeresis cracks (Fig. 10B,C) are relatively abundant in facies 6 and soft-sediment deformation structures are locally observed. Sedimentary structures observed within sandstones include

horizontal (plane-parallel) lamination, wave ripples, current ripples, and combined flow ripples (Fig. 10C, G). The degree of bioturbation is generally low but variable (BI 0-4), with a few intensely bioturbated levels. A monospecific trace fossil suite consisting of *Chondrites* is observed in the dark grey laminated mudstones, whereas sporadic diminutive forms of *Palaeophycus*, *Planolites* (Fig. 10B,C), *Lockeia*, *Teichichnus* (Fig. 10B), *Rhizocorallium* and *Rosselia* are present in heterolithic intervals. In wireline logs, facies 6 is characterised by consistently high and relatively irregular GR log responses and a large positive separation between the NP and BD curves. The base is marked by an abrupt increase in GR log response. Facies 6 is replaced upward by facies 5 and the transition is marked by the start of a gradual, but relatively rapid upward decrease in the separation between the NP and BD curves, accompanied by a gradual decrease in GR response.

Interpretation. The fine-grained sediments and the sedimentary structures of facies 6 suggests a depositional environment characterised by relatively low energy levels, with deposition both from suspension and weak unidirectional and oscillatory traction currents. The upwards vertical stratigraphic association with delta front (facies 5), floodplain/delta plain (facies 4), and fluvial channel (facies 3) deposits point to a deltaic setting with active fluvial input, and facies 6 is accordingly interpreted as prodelta deposits. The low-abundance and low-diversity trace fossil suite, which compares with a highly impoverished expression of the *Cruziana* ichnofacies (MacEachern et al., 2007), is consistent with this interpretation, and reflect physio-chemical stresses caused by relatively high sedimentation rates and salinity fluctuations due to high freshwater input (Coates and Maceachern, 2007). Salinity fluctuations are also indicated by the common presence of syneresis cracks. The dark grey colour and the monospecific *Chondrites*-assemblage observed in some of the mudstones indicate periods of slightly depleted oxygen levels in the bottom sediment (Bromley and Ekdale, 1984). The preservation of normal-graded beds is taken to indicate deposition from sustained hyperpycnal density underflows generated during river floods (Mulder et al., 2003; Bhattacharya & MacEachern, 2009), and hence mark proximity to the river mouth.

5.9 FACIES 7 – OFFSHORE

Description. This facies consists of grey, dark grey and brownish silty mudstones (Fig. 11), locally sideritic and pyritic, observed in the Fuglen Formation. The mudstones are intensely bioturbated (BI 4-6) with a trace fossil assemblage including *Asterosoma*, *Chondrites*, *Helminthopsis*, *Phycosiphon*, *Terebellina* and *Zoophycos*. Rare belemnites are also observed. The base of facies 7 is erosional towards facies 8, and is marked by an abrupt change in petrophysical log signatures including a distinct increase in GR response.

Interpretation. Based on the dominance of mudstones, the high degree of bioturbation and the presence of marine body fossils, facies 7 is interpreted to have accumulated from suspension

below storm wave base in a well-oxygenated offshore marine environment. The trace fossil assemblage compares with a distal expression of the *Cruziana* ichnofacies (MacEachern et al., 2007) commonly associated with soft and cohesive muddy substrates under quiescent marine conditions.

5.10 FACIES 8 – TRANSGRESSIVE SHELF

Description. This facies comprises a 15-20 cm thick interval observed at the junction between the Realgrunnen Subgroup and the Fuglen Formation in wells 7122/7-2 and 7122/7-3 (Fig. 11A) where it abruptly overlies deposits of facies 2. The base of facies 8 consists of a thin (<10 cm) lag of polymictic matrix-supported conglomerates with rounded phosphate and quartz pebbles in a medium-grained sandstone matrix. These are replaced upward by white and light brown carbonates with undulating sub-horizontal lamination. Relatively small, sharp-walled, unlined, vertical to sub-vertical burrows or borings are present within the carbonates in 7122/7-2, immediately below the erosive upper contact with facies 7 and the Fuglen Formation. The burrow fills consist of mudstones comparable to those of the overlying facies.

Interpretation. The deposits of facies 8 are interpreted to have accumulated on a sediment-starved marine shelf during overall transgression. The conglomerate at the base is interpreted as a transgressive lag, and the laminated carbonates at the top of facies 8 may represent early diagenetic hardgrounds characteristic of omission surfaces (Bromley, 1975). The interpreted transgressive nature is consistent with the stratigraphic position between fully terrestrial fluvial braidplain deposits (facies 2) below and offshore marine deposits (facies 7) above. The burrows at the top of facies 8 appear to be passively filled, suggesting the substrate was at least partly lithified at the time of excavation. It therefore probably represents one of the substrate controlled suites *Glossifungites* or *Trypanites* ichnofacies (MacEachern et al., 2007). These suites commonly delineate erosion and omission surfaces that may have major sequence stratigraphic significance (MacEachern et al., 1992; Pemberton et al., 2004).

5.11 ALLUVIAL ARCHITECTURE

Within the Fruholmen Formation, two distinct intervals are distinguished based on lateral and vertical channel deposit proportions (CDP). The intervals are informally referred to as the 'lower' (24-54 m thick) and 'upper' (9-37 m thick) intervals and both are characterised by channel density maxima at their bases where fluvial sandstones appear to be laterally interconnected (i.e., multilateral) and locally include amalgamated, multi-storey channel complexes. Upwards, channel deposits become finer-grained and single storey, increasingly isolated in floodplain/delta plain fines and locally show evidence of tidal influence. With reference to sequence stratigraphic models developed for non-marine strata (e.g., Shanley & McCabe, 1991, 1993, 1994; Wright & Marriott,

1993; Olsen et al., 1995), both intervals are interpreted as lower rank (i.e., high frequency) sequences. The amount of erosion at the base of the two sequences appears to be limited. However, incision on a width and depth scale greater than that of the associated channels is suggested at the base of the 'upper' interval in well 7122/7-6. Here, the 'lower' interval is only 24 m thick and is lacking the mud-rich upper part observed in the remaining wells.

Superimposed on the internal architectural trends of the two intervals, is a consistent upward increase in CDP observed in all investigated wells (Table 3), from an average of 0.29 in the 'lower' interval to 0.53 in the 'upper' interval. Although CDP values may be considered artificially high where the Tubåen Formation has eroded into the 'upper' interval (e.g. well 7122/7-3, CDP=0.72), the general trend is apparent in the well-to-well correlation (Fig. 12). Within the 'upper' interval a second conspicuous trend is also evident. Here, maximum abundance of channel deposits and high stacking densities are seen in the two central wells (7122/7-6, CDP=0.81; 7122/7-5A, CDP=0.45) where two potential multistorey channel belts, each up to 10 m thick, are distinguished at the base of the sequence. When traced laterally into adjacent wells, the number of individual channel units and channel stacking density decreases. This points toward a tendency for rivers to be funnelled through the central part of the Goliat field during deposition of the 'upper' interval. The upward increase in CDP is interpreted as the results of an overall temporal reduction in accommodation rates during deposition of the Fruholmen Formation (e.g., Bridge and Leeder, 1979) which could be attributed to reduced subsidence rates and/or progradation of the system. Lateral variations in abundance and channel stacking density seen within the 'upper' interval, may indicate that also spatial variations in accommodation that lead to partial confinement of channels within restricted parts of the floodplain were notable in the Goliat Field area at this stage.

The braided fluvial deposits of the overlying Tubåen Formation are characterised by multiple internal scour surfaces, a lack of intervening mudstones and siltstones, and overall coarser grained sandstones than observed in the Fruholmen Formation. Equivalent changes in alluvial architecture were also noted at the Fruholmen-Tubåen boundary by Ryseth (2014) who credited this change to a regional decrease in subsidence rates coupled with rejuvenation of sediment sources to the south and increased fluvial discharge due to a transition into more humid climates around the Triassic–Jurassic boundary.

5.12 FACIES DISTRIBUTION AND KEY SEQUENCE STRATIGRAPHIC SURFACES

A well-to-well correlation and fence diagram showing the spatial distribution of facies and sequence stratigraphic surfaces recognised within the Realgrunnen Subgroup in the Goliat Field area is presented in Fig. 12. The facies interpretations and sequence stratigraphic surfaces (SB 1.1, SB 2.1 and SB 3.1; Fig. 12) outlined in this study are generally consistent with previous studies of the

Realgrunnen Subgroup in the southwestern Barents Sea (Berglund et al., 1986; Bugge et al., 2002; Gjelberg et al., 1987; Henriksen et al., 2011; Johannessen and Embry, 1989; Mørk et al., 1989; Nøttvedt et al., 1993; Ryseth, 2014; Van Veen et al., 1993; Worsley et al., 1988). The contact with the underlying Snadd Formation in the Goliat field represents a major marine incursion (i.e., the early Norian transgression; Worsley et al., 2008; Henriksen et al., 2011) and is recorded in the wireline logs by an abrupt increase in gamma ray response and a large positive separation between bulk-density and neutron-porosity curves. The surface is indicated as a maximum flooding surface (MFS) in Fig. 12 (e.g. Glørstad-Clark et al., 2010). An underlying sequence boundary (SB 1.1) is indicated in Fig. 12 to be somewhere within the uppermost Snadd Formation (e.g. Johannessen & Embry, 1989; Van Veen et al., 1993). Within the Fruholmen Formation, a succession of prodelta deposits (facies 6; 23-33 m thick) is developed above the MFS, which grade into and alternate with delta front deposits (facies 5). Above the delta front deposits, a characteristic delta-top succession (36-69 m thick) composed of floodplain/delta plain deposits (facies 4) is developed and is intersected by a network of fluvial channels (facies 3a) and tide-influenced distributary channels (facies 3b). Accordingly, the Fruholmen Formation in the Goliat field is interpreted to record widespread delta progradation and re-establishment of fluvial dominated delta plains following the early Norian transgression. Based on the internal variations in channel deposit proportions noted in section 5.11, two low rank (high-frequency) sequences bounded below by SB 1.2 and SB 1.3, respectively, are here defined within the delta-top succession (Fig. 12).

The transition into the overlying Tubåen Formation (4-18 m thick) is abrupt and clearly erosional. The Tubåen Formation, which comprises fluvial braidplain deposits (facies 2) locally overlying distal alluvial fan deposits (facies 1), record a notable shift in sediment calibre (e.g., grain size and sorting), alluvial style and architecture, and a significant basinward shift in facies compared to the Fruholmen Formation and the boundary between the two defines SB 2.1. The braidplain deposits of the Tubåen Formation are capped by a thin, calcareous horizon, interpreted as a mature palaeosol, indicative of prolonged subaerial exposure and non-deposition. These are in turn unconformably overlain, locally by a thin interval of transgressive shelf deposits (facies 8), and offshore mudstones (facies 7) of the Fuglen Formation. The upper boundary of the Tubåen Formation defines SB 3.1, and the sequence boundary is suggested to have formed by a subaerial unconformity which has subsequently been modified during transgression (i.e., ravinement). The age and stratigraphic affiliation of transgressive shelf deposits above the Tubåen Formation are uncertain due to a lack of unambiguous biostratigraphic data. The abrupt lower and upper contacts and the marked change in facies between these and both under- and overlying deposits, however, may suggest that both boundaries record appreciable sedimentary breaks. Similar phosphate-

bearing conglomerates and condensed horizons have been reported both from Toarcian–Bajocian/Bathonian strata of the Stø Formation (Berglund et al., 1986; Bugge et al., 2002; Gjelberg et al., 1987; Olausen et al., 1984) and correlative deposits in Svalbard (Bäckström and Nagy, 1985; Rismyhr et al., in review). The transgressive shelf deposits may therefore either be interpreted as an extremely condensed expression of the Stø Formation, or more plainly as transgressive deposits developed at the base of the overlying Fuglen Formation. Regardless of their stratigraphic affiliation, the transition from the Tubåen Formation into the Fuglen Formation overall reflects a major lacuna spanning the ?late Rhaetian–early Callovian, and a significant transgression with a return to open marine sedimentation in the late Middle Jurassic.

6. SEISMIC EXPRESSION OF FAULTING

The seismic expression of the Late Triassic and Jurassic successions in the Goliat area are presented in Fig. 5 where the seismic–well tie is based on well 7122/7-3 (location shown in Fig. 3).

6.1 Seismic observations

The contact between the base Fruholmen Formation of the Realgrunnen Subgroup and the underlying Snadd Formation of the Storfjorden Subgroup is marked by a zero-crossing between two prominent reflectors (Fig. 13). Within the Realgrunnen Subgroup the contact between the Fruholmen Formation and the overlying Tubåen Formation, while easily discernible in the core analysis (section 5), is not sharply defined in seismic. The Triassic succession as a whole is shown by Mulrooney et al. (2017) to thin towards the GT1 segment of the TFFC. In the Realgrunnen Subgroup, minor package thickening is observed within depo-centres north and south of the Goliat crest (Fig. 13B) which shows thinner strata up to and including the Lower Cretaceous Kolje Formation. The Realgrunnen Subgroup also shows some minor thickening adjacent to subsidiary faults affecting the Goliat anticline (Fig. 13C to F). These minor wedges also exhibit sharp up-dragged geometries similar to those described on the GT1 master fault by Mulrooney et al. (2017). A zero-crossing marked by an additional strong seismic reflector delineates the boundary between the Realgrunnen Subgroup and the Jurassic Package (Fig. 5 and Fig. 13C to F). The Jurassic and Lower Cretaceous package shows the most developed thickening of packages towards faults whereas the above-lying Cretaceous Kolmule and Kolje formations (undifferentiated) show sag geometries.

6.2 Seismic interpretation

The thinning of the Triassic succession towards the TFFC can be credited to two factors, 1) the Goliat field overlies a basement block (Mulrooney et al., 2017) which has experienced less subsidence than the greater Hammerfest Basin area, and as such did not generate the same volume

of accommodation space, and 2) the Nordmela and Stø formations (Realgrunnen Subgroup) are missing across the Goliat anticline. The nature of this missing strata, i.e., erosion, non-deposition or condensed is hard to determine due to uncertainty regarding the age of the Realgrunnen Subgroup in the SW Barents Sea (Olaussen et al., 2010). The identification of facies 8 herein (section 5), however, may favour a condensed sequence scenario, although this interpretation is ambiguous.

The minor wedge geometries adjacent to faults in the Realgrunnen Subgroup are consistent with an initial small-scale rift event in the Late Norian?–Rhaetian, although the possibly condensed nature of the upper Tubåen Formation would mask clear seismic signatures of fault activity. The up-dragged geometries in the hanging walls of these faults are consistent with fault propagation monoclines, which were subsequently breached.

Given the missing Nordmela and Stø formations, the top Realgrunnen Subgroup is interpreted as a mid-Jurassic regional unconformity (e.g., Faleide et al., 1993; Worsley, 2008; Henriksen et al., 2011) and marks the onset of the main Mesozoic phase of rifting, which continued into the lower Cretaceous Knurr Formation. The more sag-shaped thick Kolmule and Kolje formations are interpreted as post rift deposits, although Mulrooney et al. (2007) suggest minor reactivations continued into the Palaeogene.

The Goliat crest (Fig. 13B) is interpreted to have formed a structural high during deposition of the Realgrunnen Subgroup through to the Lower Cretaceous (early Barremian to Aptian) although minor variations in subsidence persist up to the Late Palaeocene to Oligocene Torsk formation.

7. FAULT ANALYSIS

Four master faults, AG1, AG2, AG3 and HR1 and seven subsidiary faults AG5, AG6, AG7, GT2, GT3, GT4 and GT5 (locations shown in Fig. 3) were subject to displacement analysis. Alan diagrams (Fig. 14) measuring fault displacement at the level of the top Realgrunnen Subgroup were produced by projecting the interpreted seismic horizons onto the fault polygons. In the EN0901 MAZ, the lack of a clear seismic reflector representing the boundary between the two formations has resulted in the subgroup being treated as a single stratigraphic unit. Due to this, fault displacement profiles and fault parallel stratigraphic thickness variations (Fig. 14) are derived from the subgroup as a whole. Displacement measurements were taken at 100 m intervals along the fault trace. The resultant Alan diagrams show displacement dissipates towards the tip points of fault traces, however the line plots produced show “saw tooth” profiles, i.e., at least two orders of displacement maxima are superimposed on the overall trend. The higher order maxima have typical, but non-systematic separation of approximately 1km, the separation of lower order maxima are more typically in the 100 to 200 m range.

Variations in the thickness of the Realgrunnen Subgroup immediately adjacent the faults are also displayed in Fig. 14. The seismic horizons that represent the top and bottom of the subgroup were projected onto the fault polygons allowing fine interval measurement (every 20 m) of the package's vertical thickness. Undulating thickness profiles are characteristic of all the analysed faults. A notable correlation between sites of increased hanging wall thickness and reduced foot wall thickness is observed.

The distribution of displacement and the variation in the thickness profiles along faults are used to identify the segment history of the faults during their early phases of growth. The occurrence of displacement maxima along through-going faults have previously been shown to represent the centres of former segments (e.g., Peacock and Sanderson, 1991; Mansfield & Cartwright, 1996; Mansfield & Cartwright, 2001; Walsh et al., 2003; Lohr et al., 2008). Thinning of the footwall profile is credited to either reduced deposition or the development of erosional catchments at the sites of footwall uplift, i.e., at the centre of fault segments (e.g., Leeder, 1991; Leeder & Jackson, 1993; Eliet & Gawthorpe, 1995; Densmore et al., 2003, 2004; Foster et al., 2010; Elliott et al., 2011). Correspondingly, thickness increases in the hanging wall are envisaged to record individual isolated basins that formed adjacent to fault segments, which is characteristic of the initial stages of rift basin development (Prosser, 1993; Childs et al., 1995; Schlische, 1995; Gawthorpe and Leeder, 2000). Sites that display displacement maxima, footwall thickness minima and hanging wall thickness maxima are highlighted in Fig. 14. Sites where all three observations coincide are confidently interpreted to mark the centres of active segments during deposition of the Realgrunnen Subgroup (yellow dashes in Fig. 14). The locations of these active segments are mapped in Fig. 15B and inform the tectonic morphology in palaeogeographic reconstructions (Fig. 16 and 17).

8. AMPLITUDE VERSUS ANGLE ATTRIBUTE ANALYSIS

Amplitude Versus Angle (AVA) attribute analysis was conducted over a 10 ms window below the top Realgrunnen Subgroup, the results of which are displayed in Fig. 15A. AVA attribute analysis has the potential to reveal subtle spatial lithology and fluid trends not readily seen from post stack amplitude analysis. The Zoeppritz (1919) equation is mathematically complex and provides limited physical insight into the variation of the reflection coefficient as a function of the incident angle. Several authors have proposed linearised approximations (Aki and Richards, 1980; Shuey, 1985; Fatti et al., 1994) to the Zoeppritz equation. Partial angle stacks with a near to far angle coverage of 10°-59° have been used as inputs to generate AVO Intercept (A) and AVO Gradient (B) using the two term Aki Richards equation (Equation 1).

$$R_{pp}(\theta) = A + B \sin^2 \theta \dots \dots \dots (1)$$

Where $R_{pp}(\theta)$ represents a P-wave reflection coefficient at a given an angle (θ). The Intercept and Gradient attributes usually provide more information when combined together, then when used independently. One of such combinations is the scaled S-wave reflectivity attribute which is proportional to the scaled difference between A and B. This attribute is less sensitive to fluid effects in reservoirs and can be used to highlight the gross depositional trends. Shales usually show a lower resistance to shearing due to inherent microfabric alignment and as a result will generally show a lower shear wave reflectivity compared to sands.

The strong positive amplitudes imaged in Fig. 15A are mapped in Fig. 15B and form expansive lobe-shaped clusters in the hanging walls of faults. These are most developed in the central part of Goliat field within the hanging wall of the AG1 fault where they form a fingered lobe (Fig. 15 B: blue box delineating Fig. 16A), adjacent to a relay zone between the central and southern GT1 fault segment (Fig. 15B: blue box delineating Fig. 16B), and in the hanging wall of the northern GT1 segment (Fig. 15B: blue box delineating Fig. 16C). Smaller less expansive areas of positive amplitudes show elongate geometries parallel to and within the hanging walls of subsidiary faults. Furthermore, discrete, ribbon-shaped areas of positive amplitudes have been interpreted, and are most developed in the hanging wall of the AG1 fault where they show sinuous and U-shaped geometries.

Based on the principals of the AVA analysis, the strong positive amplitudes in Fig. 15A represent gross sand prone areas, the geometries of which provide insight into the depositional elements of the Realgrunnen Subgroup as outlined in Fig. 15B. Palaeogeographic interpretations of key sand bodies (highlighted by blue boxes in Fig. 15B) are given in Fig. 16. Due to the erosional nature of the base Tubåen Formation, and its absence in wells 7122/7-4S, 7122/7-1 and 7122/7-5A, the AVA attribute map (Fig. 15A) likely images sedimentary features from both the Tubåen Formation and the underlying Fruholmen Formation (created from a 10 ms window). Consequently, the interpretation of gross sand prone areas and channelised features in Fig. 15 is an amalgamation of both formations.

The large lobe-shaped clusters of positive amplitudes, e.g., in the hang walls of GT1 (a) and GT1 (b) are envisaged to represent alluvial fans (Fig. 16C) as encountered in well 7122/7-3. The fingered lobe in the center of Fig. 15B appears to fan from a relay zone between the eastern tip-point of AG1 and GT2 (Fig. 16A) and is consistent with the observation of increased channel density from well logs (section 5.11). The more elongate lobes or ribbons of positive amplitudes, e.g., within the hanging walls of AG1, AG2 and some GT subsidiary faults, are interpreted as stacked or

amalgamated channel facies (Fig. 16B). Their occurrence within hanging walls and their elongate geometries parallel to faults suggests they have been influenced by tectonic topography, i.e., they display axial drainage. The more patchy positive amplitudes adjacent to faults may represent small alluvial fans whereas the discrete sinuous bodies likely represent channels and associated ox-bow lakes. The curvilinear subsidiary faults, north of AG1 (Fig. 15B), appear to have no influence on channel orientation.

9. DISCUSSION

9.1 TECTONIC CONTROL ON SEDIMENTATION IN THE GOLIAT FIELD

The synthesis of sedimentological, fault and AVA analysis herein has allowed informed palaeogeographic reconstructions to be generated for the Realgrunnen Subgroup in the Goliat field. We propose depositional models for both formations in the EN0901 MAZ area (Fig. 17). We argue that fault activity influenced the deposition of the Realgrunnen Subgroup, modifying the equilibrium profiles of continental to coastal plain environments, and is especially notable during the deposition of the Tubåen Formation. The faults shown in Fig. 17 are interpreted to have been active during deposition as deduced from fault analysis (section 7; Fig. 14), and had an influence on sedimentary architecture (Fig. 15 and Fig. 16).

Facies identified within the Fruholmen Formation indicate an overall regressive unit deposited in shallow marine, deltaic and fluvial environments, with floodplains established throughout the study area by the Norian–Rhaetian. Despite the fact that no sedimentary features diagnostic of lateral accretion or point bar deposits were observed in the fluvial deposits (facies 3), the overall depositional environment (and particularly the ‘upper interval’) is consistent with the ox-bow shaped and meandering channel features observed in the AVA map (Fig. 15A). As such, these features are inconsistent with the braidplain/alluvial fan environments interpreted for the overlying Tubåen Formation.

The strong spatial association of individual channel features and ribbons of gross sand prone areas identified in the AVA analysis map (Fig. 15), especially within the hanging walls of the AG1 and AG2 fault systems, suggests fault-related subsidence, and uplift, influenced drainage systems. In this scenario we suggest that river/distributary channels migrated or avulsed towards the axis of maximum subsidence, i.e., parallel to the structural strike (e.g., Bridge and Leeder, 1979; Miall et al., 1981). We interpret the more ribbon-like features as channel deposits where drainage became increasingly confined by continued tilting as addressed by Alexander & Leeder (1987), Gupta et al. (1999), Young et al. (2002) and Garcia-Garcia et al. (2006). This interpretation is supported by a

lateral variation in channel deposit densities in the upper part of the Fruholmen Formation (Table 3; section 5.12) which may reflect some differential movements already at this time. Discernment of channel affinity in Fig. 15 to either the Fruholmen Formations or the Tubåen Formation is difficult (AVA interval samples both formations; section 8), however, the patchy distribution of the Tubåen Formation (only present in some wells) suggests, at least some of these features are affiliated to the former.

More robust evidence of fault activity is discernible from the Tubåen Formation, which is preserved in three out of the six investigated wells and represents braidplain deposits (facies 2). In addition, texturally immature sandstones with scattered gravel and pebbles in well 7122/7-3, are interpreted as distal alluvial fan deposits. Both facies suggest fully terrestrial environments. This change in depositional environments from the underlying Fruholmen Formation suggests a regressive event caused by a fall in relative sea level, but also likely reflects increase in sediment supply due to rejuvenation of more proximal hinterlands or increasingly humid climates (e.g. Ryseth, 2014), discussed below (section 9.2).

The occurrence of alluvial fan deposits in well 7122/7-3 coincide with the large sand prone bodies identified in the AVA attribute map (Fig. 15). We interpret these sand bodies to represent texturally immature alluvial fans that were sourced locally from uplifted foot walls of active faults (Fig. 16). This interpretation is supported by the variations in the Realgrunnen Subgroup hanging wall and footwall thickness profiles immediately adjacent to the faults (section 7; Fig. 14). We interpret the general correlation of fault displacement maxima, footwall thickness minima and hanging wall thickness maxima to represent syn-kinematic footwall erosion, and preferential deposition in isolated sub-basins along a segmented, immature fault system (e.g., Peacock and Sanderson, 1991; Schlische, 1995; Mansfield & Cartwright, 1996, 2001; Walsh et al., 2003; Lohr et al., 2008). This interpretation is consistent with the initial stages of rifting in a continental setting as described by Gawthorpe & Leeder (2000). In this scenario, the texturally immature nature of the alluvial fan deposits is explained by short transport distances of material derived from semi-circular drainage catchments that develop in the footwalls of active fault segments (Leeder, 1991; Leeder & Jackson, 1993; Eliet & Gawthorpe, 1995; Densmore et al., 2003, 2004; Foster et al., 2010; Elliott et al. 2011). The catchments develop due to foot wall uplift that takes place contemporaneously, and in equilibrium to hanging wall subsidence (Barr, 1987; Wernicke & Axen, 1988; Yielding, 1991; Long & Imber, 2010).

The aforementioned spatial association of the alluvial fans with the major faults in the Goliat area, i.e., GT1 (a) and (b) as depicted in Fig. 16C and Fig. 17, suggests that during the late Norian to Rhaetian, sediment entered the Hammerfest Basin via point sources, i.e., escarpments in faults and

at relay zones between adjacent fault segments (e.g., Gupta et al., 1999; Gawthorpe & Leeder, 2000). A relay zone point source is also proposed for the alluvial fan within the hanging wall of the AG1 and the GT2 faults. In our model, (Figs. 16 and 17) we also suggest fluvial systems entered the Hammerfest Basin at relay zones between active GT1 fault segments and that axial drainage was a feature of the Tubåen Formation.

The Realgrunnen Subgroup comprises the upper producing reservoir unit in the Goliat field, while the Kobbe Formation forms the lower. More recently, the Snadd Formation has been investigated as a reservoir unit. Furthermore, hydrocarbons have also been discovered in the Klappmyss Formation. The determination of axial drainage, stacked channel geometries and alluvial facies herein can give insight into reservoir extent, connectivity and properties (Bridge and Leeder, 1979; Miall et al., 1981; Gupta et al., 1999; Leeder, 1993; Young et al., 2002; Garcia-Garcia et al., 2006; Longhitano et al., 2015). In addition, the identification of gross sand prone areas by AVA in combination with detailed knowledge of the reservoir attitude and fault architecture (Leutscher, 2013; Mulrooney et al., 2017) may allow identification of smaller reservoir compartments within the formation.

9.2 DRIVING MECHANISMS AND REGIONAL CONTEXT

To date, three major post-Caledonian tectonic phases have been identified in the Hammerfest Basin, i.e., in the Late Devonian to Middle Permian, Middle Jurassic to Early Cretaceous times and during the Cenozoic (Rønnevik et al., 1982; Gabrielsen, 1984; Faleide et al., 1984, 1993; 2008; Dengo & Røssland, 1992; Riis et al., 1986; Gudlaugsson et al., 1998; Worsley, 2008). The identification of a phase of extension during the Rhaetian is somewhat anomalous as the late Triassic in the SW Barents shelf is usually characterised by regional subsidence, tectonic quiescence, and deposition of large siliciclastic sediment volumes (Nøttvedt et al., 1993; Faleide et al., 2008; Riis et al., 2008; Worsley, 2008; Glørstad-Clark et al., 2011; Høy & Lundschieen, 2011). Local zones of Triassic fault activity, however, have been identified on and near the Loppa High Fault System (Gabrielsen, 1984; Dengo & Røssland, 1992; Gudlaugsson et al., 1998; Bjøkesett, 2010), in the Hoop Graben (Mahajan et al., 2014), and on eastern Svalbard (Anell et al., 2013; Osmundsen et al., 2014).

We discuss two synchronous tectonic episodes possibly responsible for the Late Triassic faulting described herein; 1) Rejuvenation of Fennoscandia to the south and/or vertical movements related to the early Cimmerian tectonic phase in northern Europe (Ziegler, 1982; Mayall, 1983; Zonenshain et al., 1990; Golonka, 2004), and; 2) a tectonic episode which could correlate to movement on the Novaya Zemlya Segment of the Pai-Khoi–Novaya Zemlya–South Taimyr fold belt (Scott et al., 2010; Drachev, 2016; Klausen et al., 2016) to the east. Furthermore, we consider

whether sediment loading from the aforementioned rejuvenation of Fennoscandia could have driven, or contributed to the fault event described herein.

Mørk & Smelror (2001) have credited a strong correlation of Triassic sequence boundaries in the circum-Arctic to the fact that during this time, these areas were located along the northern palaeo-margin of the Pangaeian supercontinent. The regional correlations may reflect eustatic changes along the palaeo-margin or simultaneous tectonic events affecting an amalgamated lithospheric plate. The Late Triassic coincided with onset of systematic changes in the continental configuration in northern Pangea, i.e., Greenland-Europe rotated counterclockwise relative to North America (Torsvik et al., 2002). The diminishing correlation throughout the remainder of the Mesozoic is expected as the Pangaeian supercontinent underwent break-up.

Relevant to this study, Embry (1997, 2011) and Mørk & Smelror (2001) identified base and near base Rhaetian sequence boundaries which can be correlated throughout Arctic regions (i.e., Sverdrup Basin, onshore Svalbard, the Barents Sea area and eastern Siberia). The boundaries are indicative of changes in depositional and tectonic regimes. In the case of the near base Rhaetian sequence boundary (Mørk & Smelror, 2001), a period of subaerial exposure and ravinement is recorded. This boundary likely correlates to the intra-Rhaetian unconformity described herein (SB2.1; Fig. 12) that marks the transition between the Fruholmen and Tubåen formation. This boundary has been traced by Ryseth et al. (2014) between the Hammerfest Basin in the SW Barents Sea, the Halten Terrace on the mid-Norwegian margin and the Viking Graben in the northern North Sea. In addition to this, the transition from the Snadd Formation to the Realgrunnen Subgroup (MFS in Fig. 12) in the southernmost Barents Sea is marked by a mineralogical change (Bergan & Knarud, 1993) and an increase in grain size. Mørk (1999), Riis et al. (2008) and Klausen et al. (2016) suggested that the increased quartz and k-feldspar content in the Realgrunnen Subgroup is likely derived from erosional products of Baltic Shield rocks to the south. Smelror et al. (2009) and Klausen et al. (2016) have argued that the western Barents Shelf became shielded from sediment input from the Uralides and Novaya Zemlya due to a major marine embayment in the Late Triassic to Early Jurassic. Alternatively, or complimentary to this, Ryseth (2014) credit the source change to an episode of Late Triassic to Early Jurassic rejuvenation of the Fennoscandian hinterlands, south of the Barents shelf, a concurrent reduction in subsidence rates in basin areas, and potentially a change to more humid climates around the Triassic–Jurassic boundary. This phase of rejuvenation is consistent with Hendriks & Andriessen (2002) and Hendriks (2003) who used fission track data to infer Late Triassic to Early Jurassic uplift along the onshore Atlantic rift margin of Northern Norway, and the Kola Peninsula, respectively. Furthermore, Paul et al., (2009) have credited provenance variation in the Keuper sandstones in Germany to rapid late Triassic uplift of the Caledonides in southern Norway.

Far field stresses related to movement on the Novaya Zemlya segment of the Pai-Khoi–Novaya Zemlya–South Taimyr fold belt (PNZST) is an additional potential tectonic driving mechanism for the Late Triassic faulting described herein. Drachev (2016) have reported that recent unpublished MCS data acquired by TGS Seismic Company in the vicinity of the western coast of Novaya Zemlya show a sharp angular unconformity at, or near the Triassic–Jurassic boundary. The author related this break to the main deformation phase of the Novaya Zemlya segment of the PNZST, as underlying this boundary, the entire sedimentary section is severely deformed. This evidence for Late Triassic to Early Jurassic tectonism in Novaya Zemlya may be consistent with Klausen et al. (2016) who proposed a young, Late Triassic to Early Jurassic magmatic provenance area to the east of the Barents Sea. Furthermore, this is in concurrence with Torsvik and Anderson (2002) who using thermal remagnetisation ages (220–230 Ma; pre-folding), constrained timing of Taimyr deformation to post-Mid Triassic to Late Triassic times, therefore showing that whilst thrusting terminated in the Urals during the Permian, crustal shortening continued in Taimyr, Novaya–Zemlya and the South Barents Sea, well into the Mesozoic and took place at brittle/high-crustal conditions. These observations are further bolstered by Otto and Bailey (1995) and Nikishin et al. (1996).

Finally, the SB2.1 intra-Rhaetian sequence boundary may partly reflect the early Cimmerian orogeny (Zonenshain et al., 1990; Golonka, 2004), where in the western Tethys area, several blocks of the Cimmerian provenance (Sengör, 1984; Sengör and Natalin, 1996) collided with the Eurasian margin. Golonka (2004) suggest this tectonic phase may have influenced the extinction of biota at the Triassic–Jurassic boundary. Evidence for this event affecting the northern Pangaeian margin is limited, although Mayall (1983) have credited this event for late Triassic (Rhaetian) syn-sedimentary deformation in shallow, dominantly freshwater lagoonal sediments in southwest Britain. In this scenario, the author credits earthquake activity related to the tectonic event and associated uplift in the north Somerset–South Wales area as the driving mechanisms for faulting and slump-folding in the section.

Whether the faulting event described herein was driven purely by tectonic forces, i.e., far field stresses from the aforementioned events or a more secondary force, i.e., loading of sediments albeit derived from vertical movements, has not been resolved. In the absence of tectonic stresses, vertical loading, along with increases in fluid pressure are the main factors in increasing fault activity in extensional systems, where the maximum compressive stress component is vertical (Lahr et al., 1976). Dengo & Røssland (1992) described the Triassic reactivation of some basement-involved normal faults in the Dia graben, east of the Loppa High. In this case, the reactivation was tentatively credited to the Uralian Orogeny and loading by westward prograding clastic sediments. Similarly, Anell et al. (2013) speculated that Late Triassic faults on Edgeøya, east Svalbard, were driven by

reactivation of deeper seated faults, and again credit the activity to far field stresses of the Uralian Orogeny. It is uncertain if sediment loading will provide sufficient vertical stresses in order to reactivate basement structures. Such mechanisms are usually responsible for thin-skinned deformation, i.e., in deltaic environments (Hooper et al., 2002; Imber et al., 2003; Morely et al., 2011). Brandes et al. (2011), however, credit reactivation of Jurassic basement faults of the Central European Basin System to far field extension caused by (in this case) an advancing ice-sheet, water and deltaic sediment loading.

In the Goliat area, a sediment loading scenario for late Norian?–Rhaetian faulting could be consistent with the aforementioned Fennoscandian rejuvenation and an increased influx of more proximal sediments to the Barents Sea. In this scenario, the shift to higher sedimentation rates and lower rates of subsidence offshore (as evident across the boundary between the Fruholmen and Tubåen formations; Ryseth, 2014) may have significantly increased the vertical load and reactivated underlying basement lineaments. SB3.1, identified in wells 7122/7-2 and 7122/7-3 at the top of the Tubåen Formation, likely marks a shift from thick regional deposition of deltaic sediments to a sediment-starved marine shelf, and possibly a mild erosional event. Cessation of this Late Triassic to Early Jurassic phase of faulting would likely have followed the waning in sedimentation, and faults would remain in stasis until renewed tectonism in the Middle Jurassic.

10. CONCLUSIONS

The synthesis of sedimentological, fault and AVA analysis herein has allowed informed palaeogeographic reconstructions to be generated for the Realgrunnen Subgroup in the Goliat field.

- The Fruholmen Formation forms an overall regressive succession composed of siliciclastic sediments deposited in pro-deltaic, delta front, floodplain/delta plain and fluvial environments, with marked vertical and lateral variations in channel stacking densities.
- The Tubåen Formation, which erosively overlies the Fruholmen Formation, includes coarse- to very coarse-grained sandstones deposited in fluvial braidplain and distal alluvial fan environments.
- The transition from the Tubåen Formation to the Fuglen Formation is marked by transgressive shelf deposits that record a major lacuna spanning the ?late Rhaetian–early Callovian and may represent an extremely condensed expression of the Stø Formation.

We present evidence that minor fault activity influenced the deposition of the Realgrunnen Subgroup.

- Subtle thickening of the Realgrunnen Subgroup is observed adjacent to subsidiary GT faults.
- Displacement analysis on faults reveals 2 orders of displacement maxima that correlate with footwall thickness minima and hanging wall thickness maxima. These undulations in thickness are interpreted to represent syn-kinematic footwall erosion, and preferential deposition in isolated sub-basins, respectively, along a segmented, immature fault system.
- AVA (Amplitude versus Angle) attribute maps reveal the positions and geometries of gross sand prone areas. These features are identified as individual meandering channels, ox-bow lakes, stacked/amalgamated channel bodies and alluvial fans. A tendency towards axial drainage suggests syn-depositional fault-related subsidence. We interpret large lobe-shaped sand bodies as texturally immature alluvial fans (supported by well log observations) that were sourced locally from uplifted footwalls of active faults.
- The spatial association of alluvial fans with major faults in the Goliat area suggests that sediment entered the Hammerfest Basin via point sources, e.g., escarpments in faults and at un-breached relay zones between adjacent fault segments.
- The main phase of fault activity is suggested to have occurred during deposition of the Tubåen Formation, although a lateral variation in channel deposit densities in the upper part of the Fruholmen Formation could be the result of weak differential movements already at this time.

The identification of a phase of extension during the Rhaetian is somewhat anomalous. We postulate a high flux of sediment entered the Hammerfest Basin and possibly relates to a phase of Fennoscandian hinterland rejuvenation, coupled with decreases in subsidence rates and shifts towards a more humid climate. Vertical loading may have reactivated basement lineaments. Alternatively or complimentary, faulting may relate to the movements on the Novaya Zemlya segment of the Pai-Khoi–Novaya Zemlya–South Taimyr fold belt and/or to the early Cimmerian tectonic phase in northern Europe.

11. ACKNOWLEDGEMENTS

We thank Eni Norge and Statoil ASA of the PL229 license for the provision of the EN0901 multi-azimuth seismic survey, petrophysical well log data and access to the Goliat well core. We thank the Goliat team for their support and contribution throughout the study. We gratefully acknowledge Schlumberger Software for the provision of Petrel E&P Software Platform, Badley Geoscience Ltd for the provision of T7 and CGG for the provision of HampsonRussel AVO analysis & modelling software. Giovanni Barreca, Sergio Longhitano and an anonymous reviewer are acknowledged for their contribution to the improvement of this manuscript. This study formed part of the Petromax Trias

North Project (grant 234152); we extend gratitude to the projects financial supporters, the Research Council of Norway and industry partners, Edison Norway, Lundin Norway, RWE Dea Norge, Statoil and Tullow Oil. The study also formed part of the Eni Norge sponsored FASENA project (RIS-ID: 10025).

12. References

Aki, K., Richards, P.G., 1980. *Quantitative Seismology, Theory and Methods*, Vol. 1 WH Freeman & Co. New York.

Alexander, J., Leeder, M.R., 1987. Active Tectonic Control on Alluvial Architecture. *Recent Dev. Fluv. Sedimentol. Recent Dev*, 243–252. doi:10.2110/pec.87.39.0243

Anell, I., Braathen, a, Olausen, S., Osmundsen, P.T., 2013. Evidence of faulting contradicts a quiescent northern Barents Shelf during the Triassic. *First Break* 31, 67–76. doi:10.3997/1365-2397.2013017

Anell, I., Braathen, A., Olausen, S., 2014. The Triassic – Early Jurassic of the northern Barents Shelf: a regional understanding of the Longyearbyen CO₂ reservoir. *Nor. J. Geol.* 94, 83–98.

Barr, D., 1987. Lithospheric stretching, detached normal faulting and footwall uplift. *Cont. Extensional Tectonics* 28, 75–94. doi:10.1144/GSL.SP.1987.028.01.07

Bergan, M., Knarud, R., 1993. Apparent changes in clastic mineralogy of the Triassic–Jurassic succession, Norwegian Barents Sea: possible implications for palaeodrainage and subsidence. *Arct. Geol. Pet. Potential, Nor. Pet. Soc. (NPF), Spec. Publ.* 2, 481–493.

Berglund, L.T., Augustson, G., Færseth, R., Ramberg-Moe, H., 1986. The evolution of the Hammerfest Basin. *Habitat Hydrocarb. Nor. Cont. Margin* 319–338.

Bjøkesett, S., 2010. Late Paleozoic-Triassic Evolution of the Paleo- Loppa High, Linked to Tectonic Events and Depositional Patterns. MSc thesis, University of Oslo.

Blair, T.C., 1999. Cause of dominance by sheetflood vs. debris-flow processes on two adjoining alluvial fans, Death Valley, California. *Sedimentology* 46, 1015–1028. doi:10.1046/j.1365-3091.1999.00261.x

Blair, T.C., McPherson, J.G., 1994. Alluvial fans and their natural distinction from rivers based on morphology, hydraulic processes, sedimentary processes, and facies assemblages. *J. Sediment. Res.* 64.

Brandes, C., Polom, U., Winsemann, J., 2011. Reactivation of basement faults: Interplay of ice-sheet advance, glacial lake formation and sediment loading. *Basin Res.* 23, 53–64. doi:10.1111/j.1365-2117.2010.00468.x

Bridge, J.S., 2006. Fluvial facies models: recent developments. *Facies Model. Revisit.* 84, 85–170. doi:10.2110/pec.06.84.0019

- Bridge, J.S., Leeder, M.R., 1979. A simulation model of alluvial stratigraphy. *Sedimentology* 26, 617–644.
- Bromley, R.G., 1975. Trace fossils at omission surfaces, in: *The Study of Trace Fossils*. Springer, pp. 399–428.
- Bromley, R.G., Ekdale, A.A., 1984. Chondrites: a trace fossil indicator of anoxia in sediments. *Science* 224, 872–875.
- Bull, J.M., Barnes, P.M., Lamarche, G., Sanderson, D.J., Cowie, P.A., Taylor, S.K., Dix, J.K., 2006. High-resolution record of displacement accumulation on an active normal fault: implications for models of slip accumulation during repeated earthquakes. *J. Struct. Geol.* 28, 1146–1166. doi:10.1016/j.jsg.2006.03.006
- Blum, M.D., Tornqvist, T.E., 2000. Fluvial responses to climate and sea-level change: A review and look forward. *Sedimentology* 47, 2–48. doi:10.1046/j.1365-3091.2000.00008.x
- Cartwright, J. a., Mansfield, C., Trudgill, B., 1996. The growth of normal faults by segment linkage. *Geol. Soc. London, Spec. Publ.* 99, 163–177. doi:10.1144/GSL.SP.1996.099.01.13
- Cartwright, J.A., Trudgill, B.D., Mansfield, C.S., 1995. Fault growth by segment linkage: an explanation for scatter in maximum displacement and trace length data from the Canyonlands Grabens of SE Utah. *J. Struct. Geol.* 17, 1319–1326. doi:10.1016/0191-8141(95)00033-A
- Childs, C., Manzocchi, T., Nicol, A., Walsh, J.J., Soden, A.M., Conneally, J.C., Delogkos, E., 2016. The relationship between normal drag, relay ramp aspect ratio and fault zone structure. *Geol. Soc. London, Spec. Publ.* 439. doi:10.1144/SP439.16
- Childs, C., Nicol, A., Walsh, J.J., Watterson, J., 2002. The growth and propagation of synsedimentary faults. *J. Struct. Geol.* 25, 633–648. doi:10.1016/S0191-8141(02)00054-8
- Childs, C., Watterson, J., Walsh, J.J., 1995. Fault overlap zones within developing normal fault systems. *J. Geol. Soc. London.* 152, 535–549. doi:10.1144/gsjgs.152.3.0535
- Childs, C., Watterson, J., Walsh, J.J., 1996. A model for the structure and development of fault zones. *J. Geol. Soc. London.* 153, 337–340. doi:10.1144/gsjgs.153.3.0337
- Coates, L., Maceachern, J.A., 2007. The ichnological signatures of river-and wave-dominated delta complexes: differentiating deltaic and non-deltaic shallow marine successions, Lower Cretaceous Viking Formation and Upper Cretaceous Dunvegan Formation, west-central Alberta, In: MacEachern, J.A., Bann, K.L., Gingras, M.K., Pemberton, S.G. (Eds.), *Appl. Ichnology*. SEPM Soc. Sediment. Geol. pp. 227-255.
- Collinson, J.D., 1996. Alluvial sediments. *Sediment. Environ. Process. facies Stratigr.* Reading, H.G. (Ed.), *Sediment. Environ. Process. Facies Stratigr.* 3rd ed. Blackwell Publ. pp. 37-82.
- Cowie, P.A., Scholz, C.H., 1992. Displacement-length scaling relationship for faults: data synthesis and discussion. *J. Struct. Geol.* 14, 1149–1156.

- Dawers, N.H., Anders, M.H., 1995. Displacement-length scaling and fault linkage. *J. Struct. Geol.* 17, 607611–609614.
- Dawers, N.H., Anders, M.H., Scholz, C.H., 1993. Growth of normal faults Displacement-length scaling.pdf. *Geology* 21, 1107–1110.
- Dengo, C.A., Røssland, K.G., 1992. Extensional tectonic history of the western Barents Sea. *Structural Tecton. Model. its Appl. to Pet. Geol.* 1, 91–107.
- Densmore, a L., Dawers, N.H., Gupta, S., Guidon, R., Goldin, T., 2004. Footwall topographic development during continental extension. *J. Geophys. Res.* 109, 1–16. doi:10.1029/2003JF000115
- Densmore, A.L., Dawers, N.H., Gupta, S., Allen, P.A., Gilpin, R., 2003. Landscape evolution at extensional relay zones. *J. Geophys. Res.* 108, 1–15. doi:10.1029/2001JB001741
- Drachev, S.S., 2016. Fold belts and sedimentary basins of the Eurasian Arctic. *Arktos* 2, 21. doi:10.1007/s41063-015-0014-8
- Eliet, P.P., Gawthorpe, R.L., 1995. Drainage development and sediment supply within rifts, examples from the Sperchios basin, central Greece. *J. Geol. Soc. London.* 152, 883–893. doi:10.1144/gsjgs.152.5.0883
- Elliott, G.M., Wilson, P., Jackson, C.A.L., Gawthorpe, R.L., Michelsen, L., Sharp, I.R., 2011. The linkage between fault throw and footwall scarp erosion patterns: An example from the Bremstein Fault Complex, offshore Mid-Norway. *Basin Res.* 24, 180–197. doi:10.1111/j.1365-2117.2011.00524.x
- Elliott, T., 1974. Interdistributary bay sequences and their genesis. *Sedimentology* 21, 611–622.
- Embry, A., 2011. Petroleum prospectivity of the Triassic–Jurassic succession of Sverdrup Basin, Canadian Arctic Archipelago. *Geol. Soc. London, Mem.* 35, 545–558.
- Embry, A.F., 1997. Global sequence boundaries of the Triassic and their identification in the Western Canada Sedimentary Basin. *Bulletin of Canadian Petroleum Geology* 45, 415–433.
- Ethridge, F.G., Wescott, W.A., 1984. Tectonic setting, recognition and hydrocarbon reservoir potential of fan-delta deposits. *Sedimentology of Gravels and Conglomerates. Memoir* 10, 217–235.
- Faleide, J.I., Gudlaugsson, S.T., Jacquart, G., 1984. Evolution of the western Barents Sea. *Mar. Pet. Geol.* 1, 123–150.
- Faleide, J.I., Tsikalas, F., Breivik, a J., Mjelde, R., Ritzmann, O., Engen, O., Wilson, J., Eldholm, O., 2008. Structure and evolution of the continental margin off Norway and the Barents Sea. *Episodes* 31, 82–91. doi:10.1016/j.strusafe.2006.11.005
- Faleide, J.I., Våagnes, E., Gudlaugsson, S.T., 1993. Late Mesozoic-Cenozoic evolution of the southwestern Barents Sea in a regional rift-shear tectonic setting. *Mar. Pet. Geol.* 10, 186–214. doi:10.1016/0264-8172(93)90104-Z

Fatti, J.L., Smith, G.C., Vail, P.J., Strauss, P.J., Levitt, P.R., 1994. Detection of gas in sandstone reservoirs using AVO analysis: A 3-D seismic case history using the Geostack technique. *Geophysics* 59, 1362–1376. doi:10.1190/1.1443695.

Foster, D., Brocklehurst, S.H., Gawthorpe, R.L., 2010. Glacial-topographic interactions in the Teton Range, Wyoming. *J. Geophys. Res. Earth Surf.* 115, 1–20. doi:10.1029/2008JF001135

Friedman, G.M., Sanders, J.E., 1978. *Principles of sedimentology*. Wiley.

Gabrielsen, R.H., 1984. Long-lived fault zones and their influence on the tectonic development of the southwestern Barents Sea. *J. Geol. Soc. London.* 141, 651–662. doi:10.1144/gsjgs.141.4.0651

Gabrielsen, R.H., Færseth, R.B., 1988. Cretaceous and Tertiary reactivation of master fault zones of the Barents Sea. *Nor. Polarinstitutt Rapp* 46, 93–97.

Gabrielsen, R.H., Færseth, R.B., 1989. The inner shelf of North Cape, Norway and its implications for the Barents Shelf-Finmark Caledonide boundary. A comment. *Nor. Geol. Tidsskr.* 69, 57–62.

Gabrielsen, R.H., Færseth, R.B., Jensen, L.N., Kalheim, J.E., Riis, F., 1990. Structural Elements of the Norwegian continental shelf. Part 1: The Barents Sea Region. *NPD- Bull.* No.6, 33 pp.

Gabrielsen, R.H., Faleide, J.I., Leever, K. a, Grunnaleite, I., 2011. Strike-slip related inversion-tectonics of the southwestern Barents Sea (Norwegian Shelf) in a plate tectonic perspective. *Geophys. Res. Abstr.* 13.

García-García, F., Fernández, J., Viseras, C., Soria, J.M., 2006. Architecture and sedimentary facies evolution in a delta stack controlled by fault growth (Betic Cordillera, southern Spain, late Tortonian). *Sediment. Geol.* 185, 79–92. doi:10.1016/j.sedgeo.2005.10.010

Gastaldo, R., G., A., Huc, A., 1995. The tidal character of fluvial sediments of the modern Mahakam River delta, Kalimantan, Indonesia. *Spec. Publ. int. Ass. Sediment.* 24, 171–181. doi:10.1016/0264-8172(96)83693-2

Gawthorpe, R.L., Colella, A., 1990. Tectonic Controls on Coarse-Grained Delta Depositional Systems in Rift Basins, in: *Coarse-Grained Deltas*. Blackwell Publishing Ltd., pp. 113–127. doi:10.1002/9781444303858.ch6

Gawthorpe, R.L., Leeder, M.R., 2000. Tectono-sedimentary evolution of active extensional basins. *Basin Res.* 12, 195–218. doi:10.1111/j.1365-2117.2000.00121.x

Gernigon, L., Brönnner, M., Roberts, D., Olesen, O., Nasuti, A., Yamasaki, T., 2014. Crustal and basin evolution of the southwestern Barents Sea: from Caledonian orogeny to continental breakup. *Tectonics* 33, 347–373. doi:doi:10.1002/2013TC003439

Glørstad-Clark, E., Birkeland, E.P., Nystuen, J.P., Faleide, J.I., Midtkandal, I., 2011. Triassic platform-margin deltas in the western Barents Sea. *Mar. Pet. Geol.* 28, 1294–1314. doi:10.1016/j.marpetgeo.2011.03.006

- Glørstad-Clark, E., Inge, J., Anders, B., Petter, J., 2010. Triassic seismic sequence stratigraphy and paleogeography of the western Barents Sea area. *Marine and Petroleum Geology* 27, 1448–1475. doi:10.1016/j.marpetgeo.2010.02.008
- Golonka, J., 2004. Plate tectonic evolution of the southern margin of Eurasia in the Mesozoic and Cenozoic. *Tectonophysics* 381, 235–273. doi:10.1016/j.tecto.2002.06.004
- Gudlaugsson, S.T., Faleide, J.I., Johansen, S.E., Breivik, A.J., 1998. Late Palaeozoic structural development of the South-western Barents Sea. *Mar. Pet. Geol.* 15, 73–102. doi:10.1016/S0264-8172(97)00048-2
- Gupta, S., Underbill, J.R., Sharp, I.R., Gawthorpe, R.L., 1999. Role of fault interactions in controlling synrift sediment dispersal patterns: Miocene, Abu Alaqa Group, Suez Rift, Sinai, Egypt. *Basin Res.* 11, 167–189. doi:10.1046/j.1365-2117.1999.00300.x
- Harvey, A.M., Mather, A.E., Stokes, M., 2005. Alluvial fans: geomorphology, sedimentology, dynamics — introduction. A review of alluvial-fan research. *Geol. Soc. London, Spec. Publ.* 251, 1–7. doi:10.1144/GSL.SP.2005.251.01.01
- Hendriks, B.W.H., 2003. Cooling and denudation of the Norwegian and Barents Sea Margin, North Scandinavia, constrained by apatite fission track and (U-Th)/He thermochronology PhD Thesis, Vrije Universiteit Amsterdam,. doi:10.13140/RG.2.1.4347.9127
- Hendriks, B.W.H., Andriessen, P.A.M., 2002. Pattern and timing of the post-Caledonian denudation of northern Scandinavia constrained by apatite fission-track thermochronology. *Geol. Soc. London, Spec. Publ.* 196, 117–137. doi:10.1144/gsl.sp.2002.196.01.08
- Henriksen, E., Bjornseth, H.M., Hals, T.K., Heide, T., Kiryukhina, T., Klovjan, O.S., Larssen, G.B., Ryseth, a. E., Ronning, K., Sollid, K., Stoupakova, a., 2011. Uplift and erosion of the greater Barents Sea: impact on prospectivity and petroleum systems. *Geol. Soc. London, Mem.* 35, 271–281. doi:10.1144/M35.17
- Holbrook, J., Scott, R.W., Oboh-lkuenobe, F.E., 2006. Base-level buffers and buttresses: a model for upstream versus downstream control on fluvial geometry and architecture within sequences. *J. Sediment. Res.* 76, 162–174. doi:10.2110/jsr.2005.10
- Holmes, A., 1965. *Principles of physical geology*, New and fu. ed. New York : Ronald Press Co.
- Hooke, R.L., 1967. Processes on arid-region alluvial fans. *The Journal of Geology* 75, 438–460.
- Hooper, R.J., Fitzsimmons, R.J., Grant, N., Vendeville, B.C., 2002. The role of deformation in controlling depositional patterns in the south-central Niger Delta, West Africa. *Journal of Structural Geology* 24, 847–859.
- Høy, T., Lundschieen, B.A., 2011. Triassic deltaic sequences in the northern Barents Sea. *Geological Society, London, Memoirs* 35, 249–260.
- Imber, J., Childs, C., Nell, P.A.R., Walsh, J.J., Hodgetts, D., Flint, S., 2002. Hanging wall fault kinematics and footwall collapse in listric growth fault systems. *J. Struct. Geol.* 25, 197–208. doi:10.1016/S0191-8141(02)00034-2

Indrevær, K., Bergh, S.G., Koehl, J.B., Hansen, J.A., Schermer, E.R., Ingebrigtsen, A., 2013. Post-Caledonian brittle fault zones on the hyperextended SW Barents Sea margin: New insights into onshore and offshore margin architecture. *Nor. Geol. Tidsskr.* 93, 167–188.

Indrevær, K., Gabrielsen, R.H., Faleide, J.I., 2016. Early Cretaceous synrift uplift and tectonic inversion in the Loppa High area, southwestern Barents Sea, Norwegian shelf. *J. Geol. Soc. London.* jgs2016-066. doi:10.1144/jgs2016-066

Indrevær, K., Gabrielsen, R.H., Faleide, J.I., 2017. Early Cretaceous synrift uplift and tectonic inversion in the Loppa High area, southwestern Barents Sea, Norwegian shelf. *J. Geol. Soc. London.* 174, 242–254. <https://doi.org/10.1144/jgs2016-066>

Jakobsson, M., Mayer, L., Coakley, B., Dowdeswell, J.A., Forbes, S., Fridman, B., Hodnesdal, H., Noormets, R., Pedersen, R., Rebesco, M., Schenke, H.W., Zarayskaya, Y.A., Accettella, D., Armstrong, A., Anderson, R.M., Bienhoff, P., Camerlenghi, A., Church, I., Edwards, M.B., Gardner, J.V., Hall, J.K., Hell, B., Hestvik, O.B., Kristoffersen, Y., Marcussen, C., Mohammad, R., Mosher, D., Nghiem, S.V., Pedrosa, M.T., Travaglini, P.G. and Weatherall, P. (2012). The international bathymetric chart of the Arctic Ocean (IBCAO) version 3.0. *Geophysical research letters*, 39. doi: 10.1029/2012GL052219

Kim, Y.S., Sanderson, D.J., 2005. The relationship between displacement and length of faults: A review. *Earth-Science Rev.* 68, 317–334. doi:10.1016/j.earscirev.2004.06.003

Klausen, T.G., Müller, R., Slama, J., Helland-Hansen, W., 2016. Evidence for Late Triassic provenance areas and Early Jurassic sediment supply turnover in the Barents Sea Basin of northern Pangea. *Lithosphere* L556.1. doi:10.1130/L556.1

Klausen, T.G., Ryseth, A.E., Helland-Hansen, W., Gawthorpe, R., Laursen, I., 2015. Regional development and sequence stratigraphy of the Middle to Late Triassic Snadd Formation, Norwegian Barents Sea. *Mar. Pet. Geol.* 62, 102–122. <https://doi.org/10.1016/j.marpetgeo.2015.02.004>

Knutsen, S.M., Vorren, T.O., 1991. Early Cenozoic sedimentation in the Hammerfest Basin. *Mar. Geol.* 101, 31–48. doi:10.1016/0025-3227(91)90061-8

Kristensen, M.B., Childs, C.J., Korstgård, J.A., 2008. The 3D geometry of small-scale relay zones between normal faults in soft sediments. *J. Struct. Geol.* 30, 257–272. doi:http://dx.doi.org/10.1016/j.jsg.2007.11.003

Lahr, K.M., Lahr, J.C., Lindh, A.G., Bufe, C.G., Lester, F.W., 1976. The August 1975 Oroville Earthquakes. *Bull. Seismol. Soc. Am.* 66, 1085–1099.

Leeder, M.R., 1991. Denudation, vertical crustal movements and sedimentary basin infill. *Geol. Rundschau* 80, 441–458. doi:10.1007/BF01829376

Leeder, M.R., Gawthorpe, R.L., 1987. Sedimentary models for extensional tilt-block/half-graben basins. *Geol. Soc. London, Spec. Publ.* 28, 139–152. doi:10.1144/GSL.SP.1987.028.01.11

Leeder, M.R., Jackson, J.A., 1993. The interaction between normal faulting and drainage in active extensional basins, with examples from the western United States and central Greece. *Basin Res.* 5, 79–102. doi:10.1111/j.1365-2117.1993.tb00059.x

Leutscher, J., 2013. Goliat Field, a step-by-step improvement of the Seismic Image, in: Production Geoscience Society of Norway, Stavanger, 06/11/2013.

Leutscher, J., Nerby, A.M., 2011. Seismic Interpretation Report, EN0901 MAZ Survey, Unpublished Eni Norge internal report.

Lohr, T., Krawczyk, C.M., Oncken, O., Tanner, D.C., 2008. Evolution of a fault surface from 3D attribute analysis and displacement measurements. *J. Struct. Geol.* 30, 690–700. doi:10.1016/j.jsg.2008.02.009

Long, J.J., Imber, J., 2010. Geometrically coherent continuous deformation in the volume surrounding a seismically imaged normal fault-array. *J. Struct. Geol.* 32, 222–234. doi:10.1016/j.jsg.2009.11.009

Longhitano, S.G., 2008. Sedimentary facies and sequence stratigraphy of coarse-grained Gilbert-type deltas within the Pliocene thrust-top Potenza Basin (Southern Apennines, Italy). *Sedimentary Geology* 210, 87–110. doi:10.1016/j.sedgeo.2008.07.004

Longhitano, S.G., Mellere, D., Steel, R.J., Ainsworth, R.B., 2012. Tidal depositional systems in the rock record: A review and new insights. *Sedimentary Geology* 279, 2–22. doi:10.1016/j.sedgeo.2012.03.024

Longhitano, S.G., Sabato, L., Tropeano, M., Murru, M., Carannante, G., Simone, L., Cilona, A., Vigorito, M., 2015. Outcrop reservoir analogous and porosity changes in continental deposits from an extensional basin: The case study of the upper Oligocene Sardinia Graben System, Italy. *Marine and Petroleum Geology* 67, 439–459. doi:10.1016/j.marpetgeo.2015.05.022

Longhitano, S.G., Telesca, D., Pistis, M., 2017. Tidal sedimentation preserved in volcanoclastic deposits filling a peripheral seaway embayment (early Miocene, Sardinian Graben). *Marine and Petroleum Geology* 87, 31–46. doi:10.1016/j.marpetgeo.2017.05.007

MacEachern, J., Raychaudhuri, I., Pemberton, S., 1992. Stratigraphic applications of the Glossifungites ichnofacies: Delineating discontinuities in the rock record. *SEPM Core Work. (Society Econ. Paleontol. Mineral.* 169–198. doi:10.1144/GSL.SP.2004.228.01.03

MacEachern, J.A., Bann, K.L., Pemberton, S.G., Gingras, M.K., 2007. The ichnofacies paradigm: High-resolution paleoenvironmental interpretation of the rock record. *Applied ichnology. SEPM Short Course Notes* 52, 27–64. doi:10.2110/pec.07.52.0027

Mackin, J.H., 1948. Concept of the graded river. *Geol. Soc. Am. Bull.* 59, 463–512. doi:10.1130/0016-7606(1948)59[463:COTGR]2.0.CO;2

Mahajan, A., Gabrielsen, R. H., Faleide, J.I., 2014. Structural Evolution using 3D Seismic of Hoop Fault Complex, SW Barents Sea Norway. *Conf. Arct. Energy Conf. Tromso, Vol. NGF Abstr. Proc. 2014, Vol 2.*

Mansfield, C., Cartwright, J., 2001. Fault growth by linkage: Observations and implications from analogue models. *J. Struct. Geol.* 23, 745–763. doi:10.1016/S0191-8141(00)00134-6

- Mansfield, C.S., Cartwright, J.A., 1996. High resolution fault displacement mapping from three-dimensional seismic data: evidence for dip linkage during fault growth. *Journal of Structural Geology* 18, 249–263.
- Marrett, R., Allmendinger, R.W., 1991. Estimates of strain due to brittle faulting: sampling of fault populations. *J. Struct. Geol.* 13, 735–738. doi:10.1016/0191-8141(91)90034-G
- Martinius, A.W., Gowland, S., 2011. Tide-influenced fluvial bedforms and tidal bore deposits (Late Jurassic Lourinhã Formation, Lusitanian Basin, Western Portugal). *Sedimentology* 58, 285–324. doi:10.1111/j.1365-3091.2010.01185.x
- Mayall, M.J., 1983. An earthquake origin for synsedimentary deformation in a late Triassic (Rhaetian) lagoonal sequence, southwest Britain. *Geol. Mag.* 120, 613–622. doi:10.1017/S001675680002776X
- Mellere, D., Mannie, A., Longhitano, S., Mazur, M., Kulausa, H., Brough, S., Cotton, J., 2017. Tidally influenced shoal water delta and estuary in the Middle Jurassic of the Søgne Basin, Norwegian North Sea: sedimentary response to rift initiation and salt tectonics. Geological Society, London, Special Publications 444, 173–213.
- Meyer, V., Nicol, A., Childs, C., Walsh, J.J., Watterson, J., 2002. Progressive localisation of strain during the evolution of a normal fault population. *J. Struct. Geol.* 24, 1215–1231. doi:http://dx.doi.org/10.1016/S0191-8141(01)00104-3
- Miall, A.D., 1981. Sedimentation and tectonics in alluvial basins., *Geol.Assoc.Can.Spec.Pap.* Geological Association of Canada, Department of Earth Sciences, University of Waterloo. doi:10.1016/0012-8252(83)90024-7
- Mørk, A., Smelror, M., 2001. Correlation and non-correlation of high order circum-arctic Mesozoic sequences. *Polarforschung* 69, 65–72.
- Mørk, A., W. K. Dallmann, H. Dypvik, E. P. Johannessen, G. B. Larssen, J. Nagy, A. Nøttvedt, S. Olausson, T. M. Pchelina, and D.W., 1999. Mesozoic lithostratigraphy. Lithostratigraphic lexicon of Svalbard. Upper Palaeozoic to Quaternary bedrock. Review and recommendations for nomenclature use. *Norsk Polarinstitutt, Tromsø*, pp. 127–214.
- Mørk, M.B.E., 1999. Compositional variations and provenance of Triassic sandstones from the Barents Shelf. *Journal of Sedimentary Research* 69, 690–710.
- Morley, C.K., King, R., Hillis, R., Tingay, M., Backe, G., 2011. Deepwater fold and thrust belt classification, tectonics, structure and hydrocarbon prospectivity: A review. *Earth-Science Reviews* 104, 41–91.
- Mulrooney, M.J., Leutscher, J., Braathen, A., 2017. A 3D structural analysis of the Goliat field, Barents Sea, Norway. *Mar. Pet. Geol.* doi:10.1016/j.marpetgeo.2017.05.038
- Nemec, W., Postma, G., 1993. Quaternary alluvial fans in southwestern Crete: sedimentation processes and geomorphic evolution, in: *Alluvial Sedimentation*. IAS Special Publication, pp. 235–276.

Nemec, W., Steel, R.J., 1984. Alluvial and coastal conglomerates: their significant features and some comments on gravelly mass-flow deposits. *Sedimentol. Gravels Conglomerates* 10, 1–31.

Nemec, W., Steel, R.J., 1988. What is a fan delta and how do we recognize it? *Fan deltas; Sedimentol. Tecton. settings.* 3–13. doi:10.1111/j.1365-2117.1988.tb00021.x

Nicol, A., Walsh, J.J., Villamor, P., Seebeck, H., Berryman, K.R., 2010. Normal fault interactions, paleoearthquakes and growth in an active rift. *J. Struct. Geol.* 32, 1101–1113. doi:10.1016/j.jsg.2010.06.018

Nikishin, A.M., Ziegler, P.A., Stephenson, R.A., Cloetingh, S.A.P.L., Furne, A.V., Fokin, P.A., Ershov, A.V., Bolotov, S.N., Korotaev, M.V., Alekseev, A.S., Gorbachev, V.I., Shipilov, E.V., Lankreijer, A., Bembinova, E.Y., Shalimov, I.V., 1996. Late Precambrian to Triassic history of the East European Craton: dynamics of sedimentary basin evolution. *Tectonophysics* 268, 23–63. doi:10.1016/S0040-1951(96)00228-4

Nøttvedt, A., Cecchi, M., Gjelberg, J.G., Kristensen, S.E., Lønøy, A., Rasmussen, A., Rasmussen, E., Skott, P.H., Van Veen, P.M., 1993. Svalbard-Barents Sea correlation: a short review. *Arct. Geol. Pet. Potential, Nor. Pet. Soc. (NPF), Spec. Publ.* 2, 363–375.

Olaussen, S., Galimberti, R.F., Grindhaug, J.K., Heskestad, B., Leutscher, J., Johnsen, E., Johnsen, S., Opsahl, E., Seldal, J. and Stensland, D., 2010. Hydrocarbon pools banked to the basin margin faults: harvesting a successful play model in the south-western Barents Sea, in: 29th Nordic Geological Winter Meeting. Abstracts and Proceedings of the Geological Society of Norway. Pp 139 -140.

Olaussen, S., Dalland, A., Gloppen, T.G., Johannessen, E., 1984. Depositional environment and diagenesis of Jurassic reservoir sandstones in the eastern part of Troms I area, in: Spencer, A.M. (Ed.), *Petroleum Geology of the North European Margin: Proceedings of the North European Margin Symposium (NEMS '83)*, Organized by the Norwegian Petroleum Society and Held at the Norwegian Institute of Technology (NTH) in Trondheim 9–11 May, 1983. Springer Netherlands, Dordrecht, pp. 61–79. doi:10.1007/978-94-009-5626-1_6

Olariu, C., Bhattacharya, J.P., 2006. Terminal Distributary Channels and Delta Front Architecture of River-Dominated Delta Systems. *J. Sediment. Res.* 76, 212–233. <https://doi.org/10.2110/jsr.2006.026>

Osmundsen, P.T., Braathen, A., Rød, R.S., Hynne, I.B., 2014. Styles of normal faulting and fault-controlled sedimentation in the Triassic deposits of Eastern Svalbard. *Nor. Pet. Dir. Bull.* 11, 61–79.

Ostanin, I., Anka, Z., di Primio, R., Bernal, A., 2012. Identification of a large Upper Cretaceous polygonal fault network in the Hammerfest basin: Implications on the reactivation of regional faulting and gas leakage dynamics, SW Barents Sea. *Mar. Geol.* 332–334, 109–125. doi:10.1016/j.margeo.2012.03.005

Otto, S.C., Bailey, R.J., 1995. Tectonic evolution of the northern Ural Orogen. *J. Geol. Soc. London.* 152, 903–906. doi:10.1144/GSL.JGS.1995.152.01.03

Øvrebø, O., Talleraas, E., 1977. The Structural geology of the Troms Area (Barents-Sea). *GeoJournal* 1, 47–54. doi:10.1007/BF00189603

- Paul, J., Wemmer, K., Wetzel, F., 2009. Keuper (Late Triassic) sediments in Germany - indicators of rapid uplift of Caledonian rocks in southern Norway. *Nor. Geol. Tidsskr.* 89, 193–202.
- Peacock, D.C.P., 1991. Displacements and segment linkage in strike-slip fault zones. *J. Struct. Geol.* 13, 1025–1035. doi:10.1016/0191-8141(91)90054-M
- Peacock, D.C.P., Sanderson, D.J., 1991. Displacements, segment linkage and relay ramps in normal fault zones. *J. Struct. Geol.* 13, 721–733. doi:10.1016/0191-8141(91)90033-F
- Pemberton, S.G., MacEachern, J.A., Saunders, T., 2004. Stratigraphic applications of substrate-specific ichnofacies: delineating discontinuities in the rock record. *Geol. Soc. London, Spec. Publ.* 228, 29–62.
- Postma, G., 1986. Classification for sediment gravity-flow deposits based on flow conditions during sedimentation. *Geology* 14, 291–294. doi:10.1130/0091-7613(1986)14<291
- Postma, G., 1990. Depositional Architecture and Facies of River and Fan Deltas: A Synthesis. *Coarse-Grained Deltas* 10, 13–27. doi:10.1002/9781444303858.ch2
- Prosser, S., 1993. Rift-related linked depositional systems and their seismic expression. *Geol. Soc. London, Spec. Publ.* 71, 35–66. doi:10.1144/GSL.SP.1993.071.01.03
- Riis, F., Lundschieen, B.A., Høy, T., Mørk, A., Mørk, M.B.E., 2008. Evolution of the Triassic shelf in the northern Barents Sea region. *Polar Res.* 27, 318–338. doi:10.1111/j.1751-8369.2008.00086.x
- Riis, F., Vollset, J., Sand, M., 1986. Tectonic Development of the Western Margin of the Barents Sea and Adjacent Areas. *Futur. Pet. Prov. World* 40, 661–675.
- Rismyhr, B., 2012. Sedimentological facies models of the lower part of the Realgrunnen Subgroup in the Goliat Field compared with outcrops, MSc Thesis, Department of Earth Science, University of Bergen.
- Roberts, D., Lippard, S.J., 2005. Inferred Mesozoic faulting in Finnmark: current status and offshore links. *Norges Geol. undersøkelse Bull.* 443, 55–60.
- Rønnevik, H., Jacobsen, H.-P., 1984. Structural highs and basins in the western Barents Sea BT - Petroleum Geology of the North European Margin: Proceedings of the North European Margin Symposium (NEMS '83), organized by the Norwegian Petroleum Society and held at the Norwegian Institute of, in: Spencer, A.M. (Ed.), . Springer Netherlands, Dordrecht, pp. 19–32. doi:10.1007/978-94-009-5626-1_3
- Rønnevik, H.C., 1981. Geology of the Barents Sea. *Pet. Geol. Cont. Shelf North-West Eur.* 395–405.
- Rust, B.R., Koster, E.H., 1984. Coarse Alluvial Deposits, in: *Facies Models*. Geological Association of Canada Toronto, pp. 53–69.
- Ryseth, A., 2014. Sedimentation at the Jurassic-Triassic boundary, south-west Barents Sea: Indication of climate change. *From Depos. Syst. to Sediment. Successions Nor. Cont. Margin* 46, 187–214. doi:10.1002/9781118920435.ch9

- Schlische, R.W., 1995. Geometry and origin of fault-related folds in extensional settings. *Am. Assoc. Pet. Geol. Bull.* 79, 1661–1678. doi:10.1306/7834DE4A-1721-11D7-8645000102C1865D
- Schumm, S.A., 1993. River Response to Baselevel Change: Implications for Sequence Stratigraphy. *J. Geol.* 101, 279–294. doi:10.1086/648221
- Scott, R.A., Howard, J.P., Guo, L., Schekoldin, R., Pease, V., 2010. Offset and curvature of the Novaya Zemlya fold-and-thrust belt, Arctic Russia. *Geol. Soc. London, Pet. Geol. Conf. Ser.* 7, 645–657. doi:10.1144/0070645
- Sengör, A.M., 1984. The Cimmeride Orogenic System and the Tectonics of Eurasia. *Geol. Soc. Am. Spec. Pap.* 195, 1–76. doi:10.1130/SPE195
- Sengör, A.M.C., Natalin, B.A., 1996. Paleotectonics of Asia: fragments of a synthesis. *Tectonics Asia* 486–640.
- Shuey, R.T., 1985. A simplification of the Zoeppritz equations. *Geophysics* 50, 609–614. doi:10.1190/1.1441936
- Smelror, M., Petrov, O. V, Larssen, G.B., Werner, C., 2009. Atlas. *Geol. Hist. Barents Sea Trondheim, Norway, Geol. Surv. Norw.*
- Soliva, R., Benedicto, A., 2004. A linkage criterion for segmented normal faults. *J. Struct. Geol.* 26, 2251–2267. doi:10.1016/j.jsg.2004.06.008
- Stemmerik, L., 2000. Late Palaeozoic evolution of the North Atlantic margin of Pangea. *Palaeogeogr. Palaeoclimatol. Palaeoecol.* 161, 95–126. doi:10.1016/S0031-0182(00)00119-X
- Taylor, A.M., Goldring, R., 1993. Description and analysis of bioturbation and ichnofabric. *J. Geol. Soc. London.* 150, 141–148. doi:10.1144/gsjgs.150.1.0141
- Trudgill, B., Cartwright, J., 1994. Relay-ramp forms and normal-fault linkages, Canyonlands National Park, Utah. *Geol. Soc. Am. Bull.* 106, 1143–1157. doi:10.1130/0016-7606(1994)106<1143:RRFANF>2.3.CO;2
- Visser, M.J., 1980. Neap-spring cycles reflected in Holocene subtidal large-scale bedform deposits: a preliminary note. *Geology* 8, 543–546.
- Walsh, J.J., Bailey, W.R., Childs, C., Nicol, A., Bonson, C.G., 2003. Formation of segmented normal faults: A 3-D perspective. *J. Struct. Geol.* 25, 1251–1262. doi:10.1016/S0191-8141(02)00161-X
- Walsh, J.J., Watterson, J., 1988. Analysis of relationship between displacement and dimensions of faults. *J. Struct. Geol.* 10, 239–247.
- Walsh, J.J., Watterson, J., 1991. Geometric and kinematic coherence and scale effects in normal fault systems. *Geol. Soc. London, Spec. Publ.* 56, 193–203. doi:10.1144/GSL.SP.1991.056.01.13
- Watterson, J., 1986. Fault dimensions, displacements and growth. *pure Appl. Geophys.* 124, 365–373. doi:10.1007/BF00875732

Wernicke, B., Axen, G.J., 1988. On the role of isostasy in the evolution of normal-fault systems. *Geology* 16, 848–851. doi:10.1130/0091-7613(1988)016<0848

Wilkins, S.J., Gross, M.R., 2002. Normal fault growth in layered rocks at Split Mountain, Utah: influence of mechanical stratigraphy on dip linkage, fault restriction and fault scaling. *J. Struct. Geol.* 24, 1413–1429.

Willemsse, E.J.M., Pollard, D.D., Aydin, A., 1996. Three-dimensional analyses of slip distributions on normal fault arrays with consequences for fault scaling. *J. Struct. Geol.* 18, 295–309.

Worsley, D., 2008. The post-Caledonian development of Svalbard and the western Barents Sea. *Polar Res.* 27, 298–317. doi:10.1111/j.1751-8369.2008.00085.x

Yielding, G., 1990. Footwall uplift associated with Late Jurassic normal faulting in the northern North Sea. *J. Geol. Soc. London.* 147, 219–222. doi:10.1144/gsjgs.147.2.0219

Young, M.J., Gawthorpe, R.L., Sharp, I.R., 2002. Architecture and evolution of syn-rift clastic depositional systems towards the tip of a major fault segment, Suez rift, Egypt. *Basin Res.* 14, 1–23. doi:10.1046/j.1365-2117.2002.00162.x

Ziegler, P.A., 1988. Post-Hercynian plate reorganization in the Tethys and Arctic-North Atlantic domains. *Triassic-Jurassic Rift.* New York, Elsevier 71.

Ziegler, W.H., Doery, R., Scott, J., 1986. Tectonic habitat of Norwegian oil and gas. *Habitat Hydrocarb. Nor. Cont. Shelf* 3–19.

Zoeppritz, K., 1919. On the reflection and penetration of seismic waves through unstable layers. *Göttinger Nachrichten*, 1 66–84.

Zonenshain, L.P., Kuzmin, M.I., Natapov, L.M., Page, B.M., 1990. Alpine-Himalayan Foldbelt within the USSR. *Geology of the USSR: A Plate-Tectonic Synthesis*, 168–198.

13. FIGURE CAPTIONS

Table 1. Stratigraphic picks and formation thicknesses in the studied wells.

Table 2. Summary of facies in the Realgrunnen Subgroup. BI – Bioturbation index, GR – Gamma ray, NP – neutron-porosity, BD – bulk density

Table 3. Alluvial architecture parameters of the Fruholmen Formation. Channel deposit proportion (CDP), measured as the thickness of channel deposits (T_c) relative to the total thickness of alluvial succession for a given interval (T), is found to increase consistently upward in all investigated wells from the ‘lower’ to the ‘upper’ interval (Fig. 12). Note that CDP values for the ‘upper’ interval may be artificially high where significant erosion has occurred, thereby preserving only the lower part of the sequence where the abundance and stacking density of distributary channels are the greatest.

Figure 1. Deformation of the rock volume surrounding fault segments influences the spatial and geometric nature of both deposition and erosion and can give insight into fault activity. Individual fault segments are elliptical in shape and accrue the greatest displacement towards the centre. This displacement gradient is accommodated by transverse folding, i.e., a subsiding hanging wall syncline and an uplifting footwall anticline. Accordingly, the centres of these transverse folds offer the largest accommodation space and topographic highs prone to erosion in hanging walls and footwalls, respectively. Within the hanging wall, thickening of sediment towards the fault suggests syn-kinematic deposition. Channels migrate towards the zone of maximum subsidence and adopt axial drainage. Displacement minima and hanging wall syn-rift thickness minima are characteristic of the tip points of faults or sites of linkage between formerly individual fault segments. In addition, sites of fault linkage often exhibit jogs in the fault trace. Continental rift settings are characterised by large relay zone fans and small, but numerous cross-fault fans. Fold axis concept is based on Schlische (1995). Depositional concepts are based on Gawthorpe and Leeder (2000).

Figure 2. (A) Bathymetric map of the Arctic Ocean showing the location of the western Barents Shelf. Sourced from Jakobsson et al. (2012). (B) Main structural elements of the south western Barents Shelf and adjacent areas modified from Faleide et al. (2010). Abbreviations: BB = Bjørnøya Basin, FSB = Fingerdjupet Sub-basin, HB = Harstad Basin, HfB-W = Hammerfest Basin West, HfB-E = Hammerfest Basin East, LH = Loppa High, MB = Maud Basin, MH = Mercurius High, NB = Nordkapp Basin, NH = Nordsel High, OB = Ottar Basin, PSP = Polheim Sub-platform, RLFC = Ringvassøy-Loppa Fault Complex, SB = Sørvestsnaget Basin, SFZ = Senja Fracture Zone, SH = Stappen High, SR = Senja Ridge, TB = Tromsø Basin, TFFC = Troms-Finnmark Fault complex, VH = Veslemøy High, VVP = Vestbakken Volcanic Province.

Figure 3. Depth structure map of the top Realgrunnen Formation with interpreted structural elements including the prominent Goliat anticline and basement involved master faults affecting the area. Faults are divided into four identifiable populations i) the Hammerfest Regional (HR) interpreted as the offshore Trollfjord-Komagelv Fault Zone trend, ii) the Goliat-Tornerose (GT), parallel to the northern TFFC segment, iii) the Alke-Goliat (AG), parallel to the southern TFFC segment and iv) the Goliat Central (GC) population, a series of small faults that truncate the Goliat crest. The master faults AG1, AG2, AG3 and GT1 form segments of the Troms-Finnmark Fault Complex. Locations of wells used in this study are also shown.

Figure 4. Generalised drainage of the Hammerfest Basin during the Rhaetian – Hettangian when the Tubåen Fm (198 – 209 Ma) was deposited showing fluvial systems draining towards the west within an east–west orientated embayment. Present day structural lineaments delineating the Hammerfest

Basin are shown in black. Also shown, the Goliat field (red and green) and the EN0901 survey outline (red). The paleo-reconstruction is based on unpublished Hammerfest Basin well data made available by ENI Norge.

Figure 5. Late Triassic and Jurassic seismic stratigraphy of the EN0901 MAZ survey established from the well completion log for 7122/7-3. The late Triassic is punctuated by an unconformity prior to deposition of the Realgrunnen Subgroup (Fruholmen and Tubåen formations). An additional regionally significant unconformity is located at the top of the Realgrunnen Subgroup. The Nordmela and Stø formations which are present throughout the southern Hammerfest basin are missing across the Goliat rollover structure.

Figure 6. Key to sedimentary logs.

Figure 7. Core photos and sedimentary logs of facies 1 (distal alluvial fan) and facies 2 (braided fluvial channels) in the Tubåen Formation. The stratigraphic position of the core photos is indicated in the logs. A) Structureless very coarse-grained, poorly sorted sandstone with siltstone clast in facies 1, 7122/7-3. B) Diffuse low-angle cross-stratification in coarse-grained sandstone of facies 1, 7122/7-3. C) Mudstone rip-up clasts accentuating low-angle cross-stratification in medium-grained sandstone of facies 2, 7122/7-3. D) Well-defined planar cross-stratification in fine- to medium grained sandstone of facies 2, 7122/7-3. E) Mottled, carbonate cemented bed with possible root casts in the upper part of facies 2, 7122/7-3. F) Very coarse-grained sandstone with large mudstone rip-up clast interpreted as channel base deposit of facies 2, 7122/7-2. G) Planar cross-stratified, medium-grained sandstone, 7122/7-2. H) Planar cross-stratified and current ripple laminated fine- to medium-grained sandstone at the top of a fining-upward unit, 7122/7-2. I) Gravel lag and cross-stratified coarse-grained sandstone at the base of the Tubåen Formation in 7122/7-6.

Figure 8. Representative core photos and sedimentary logs of facies 3 in the Fruholmen Formation. A) Core section showing fluvial channel deposits (facies 3b) with abandonment fill overlain by tide-influenced distributary channel deposits (facies 3b). The base and top of the cored section is at the lower right and upper left respectively. B) Details of tide-influence distributary channel deposits (facies 3b) with well-defined single and paired drapes of mud and organic debris on cross-strata foresets, 7122/7-1. C) Fine-grained planar cross-stratified sandstone with mud-drapes in facies 3b, 7122/7-2. D) Heterolithic interval with climbing current ripples, interpreted as the abandonment fill of a fluvial channel (facies 3a), 7122/7-2. E) Fine-grained planar cross-stratified sandstone with mud drapes and interbedded mud-laminae (facies 3b), 7122/7-2. F) Medium-grained cross-stratified sandstones of facies 3a, 7122/7-6. G) Fine- to medium-grained planar cross-stratified sandstone of

facies 3b with well-defined cm-thick mud drapes accentuating tangential cross-strata set bases, 7122/7-4S.

Figure 9. Representative core photos and log sections of facies 4 in the Fruholmen Formation. A) Brownish mudstones overlain by carbonaceous dark grey mudstones in 7122/7-6. B) Current-ripple laminated fine-grained sandstone with escape traces (*fu-fugichnia*) in 7122/7-2. C) Current ripple and plane parallel laminated very fine-grained sandstone in 7122/7-2. D) Massive grey mudstone with coal/plant fragments, 7122/7-2. E) Massive brown mudstone with coal fragments and possible rootlets, 7122/7-4S. F) Sharp, erosively based fine-grained sandstone, interpreted as crevasse channel deposit, 7122/7-4S. G) Upward-coarsening, bioturbated very fine- to fine-grained sandstone in 7122/7-2. H) Very fine-grained sandstone with rootlets, overlain by coal in 7122/7-4S.

Figure 10. Delta front (facies 5) and prodelta deposits (facies 6) in the Fruholmen Formation. A) Core section showing heterolithic deposits of facies 6 in 7122/7-1. Base and top of the cored section is to the lower right and upper left, respectively. B) and C) Details of prodelta deposits (facies 6) in 7122/7-1 showing interbedded mudstone, siltstone, and very fine-grained sandstone, with common syneresis cracks, rare bioturbation and occasional wave ripples. D) Core section from 7122/7-2 showing alternating deposits of facies 5 and 6. E) Root casts in fine-grained sandstone at the top of a distributary mouth bar of facies 5 in 7122/7-1. F) Plane-parallel and low angle cross-lamination in very fine-grained sandstone of facies 5 in 7122/7-2. G) Sand-rich heterolithic deposits of facies 6 in 7122/7-1 displaying thin sandstones with wave ripples and combined-flow ripples separated thin, weakly bioturbated mudstones. H) Combined flow ripples in very fine-grained sandstone of facies 5 in 7122/7-2. I) Plane-parallel and low-angle cross-laminated very fine-grained sandstone of facies 5 with rare wave ripples in 7122/7-1. *sy-syneresis cracks, Pa-Palaeophycus, Pl-Planolites, Te-Teichichnus*

Figure 11. Core photographs and sedimentary logs illustrating offshore (facies 7) and transgressive shelf (facies 8) deposits observed at the boundary between the Realgrunnen Subgroup and the Fuglen Formation. A) Matrix supported conglomerate with phosphate (Ph) and quartz-pebbles (Qz) overlain by carbonate with wavy lamination at the top of the Realgrunnen Subgroup, facies 8 in 7122/7-2. Note passively filled burrows attributed to the *Glossifungites/Trypanites* ichnofacies protruding down from the sharp boundary towards the Fuglen Formation. B) Intensely bioturbated silty mudstones of facies 7 in the Fuglen Formation, 7122/7-3. *As-Asterosoma, He-Helminthopsis, Ph-Phycosiphon*

Figure 12. Well-to-well and fence diagram correlation of the investigated Goliat Field wells. SB – sequence boundary, MFS – maximum flooding surface

Figure 13. (A) Composite seismic transect of the GT1 hanging wall. Interpreted in (B). The transect parallels the fault trace and shows the geometry of packages immediately adjacent to the fault. The Goliat crest is clearly imaged and acts as a divide between two Mesozoic fault controlled depocentres. Package thickening, indicative of fault controlled subsidence, develops in the Realgrunnen Subgroup and becomes more pronounced up section. (C,E) Key seismic profiles transecting the EN0901 MAZ survey, X – X' trends perpendicular to AG faults, Y – Y' trends perpendicular to GT faults. (D,F) Expanded view of seismic interpretations showing fault architecture affecting the Realgrunnen Subgroup, with minor growth wedging and hanging wall drag geometries highlighted. Note high population of minor faults contained within and just below the Realgrunnen Subgroup, consistent with early stages of rifting.

Figure 14. Realgrunnen Subgroup displacement profiles for four master faults, AG1, AG2, AG3 and HR1 and seven subsidiary faults AG5, AG6, AG7, GT2, GT3, GT4 and GT5, locations shown in figure 3. Two orders of displacement peaks, or maxima are recognised. Also shown: hanging wall and footwall thickness profiles for the Realgrunnen Subgroup. Hanging wall thickness maxima and foot wall minima are highlighted and likely mark sites of syn-depositional segment activity where they correlate.

Figure 15. A) Scaled S-wave reflectivity attribute map produced from a 10 ms amplitude extraction window below the top of the Realgrunnen Subgroup (Tubåen Fm). Individual sinuous channelised features and ox-bow lakes are imaged by strong positive amplitudes. More clustered strong positive amplitudes represent gross sand-prone areas i.e., stacked or amalgamated channel bodies, deltaic lobes or alluvial fans. Weaker positive and negative amplitudes represent increasingly mud prone facies, i.e., floodplain/delta plain deposits. B) Interpretation of sand-prone facies distribution in relation to active faults during the Rhaetian. Sediment point sources and routing directions highlighted by black and white arrows, respectively. Blue rectangles highlight areas subject to paleogeographic reconstructions in figure 17.

Figure 16. Paleogeographic reconstructions of key zones where fault-related geomorphology interacts with and routes sediments during the Rhaetian. Locations highlighted by blue rectangles in figure 15.

Figure 17. Summary of depositional environments and fault interaction during deposition of the Fruholmen Formation (bottom) and the Tubåen Formation (top). The Fruholmen Formation is

interpreted to include deltaic and fluvial deposits. Minor fault activity and axial drainage is envisaged at this stage. Relay ramps between unlinked segments of the GT1 fault provide point sources for regional fluvial systems to enter the Hammerfest Basin. The Tubåen Formation includes braidplain deposits with alluvial fans derived locally from uplifted footwalls.

ACCEPTED MANUSCRIPT

Well	<u>Formation tops (m MD)</u>				<u>Thickness (m)</u>		Realgrunnen Subgroup
	Snadd	Fruholmen	Tubåen	Fruholmen	Tubåen		
7122/7-1	1202	1102*	-	100	0	100	
7122/7-2	1198	1083	1077*	115	6	121	
7122/7-3	1180	1105	1087*	75	18	93	
7122/7-4S	1244	1177*	-	67	0	67	
7122/7-5A	1280	1181*	-	99	0	99	
7122/7-6	1206	1131	1122*	75	9	84	

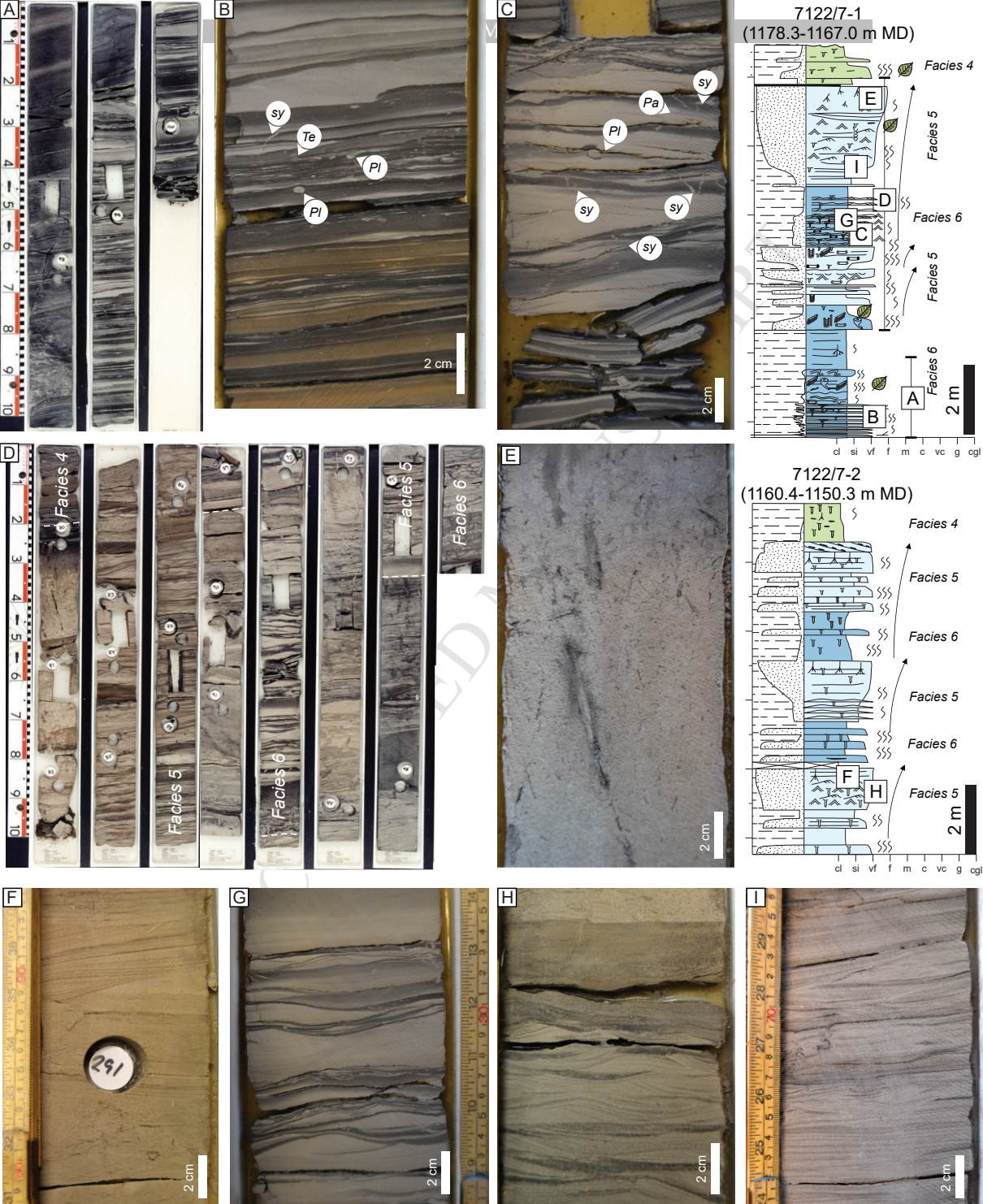
*Top Realgrunnen Subgroup

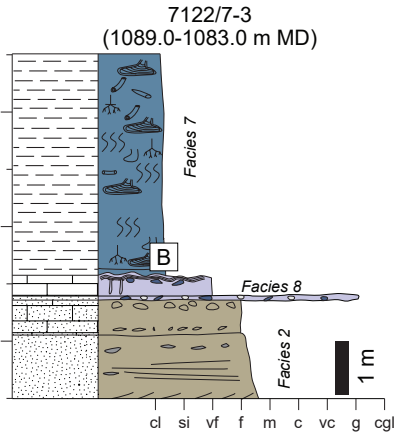
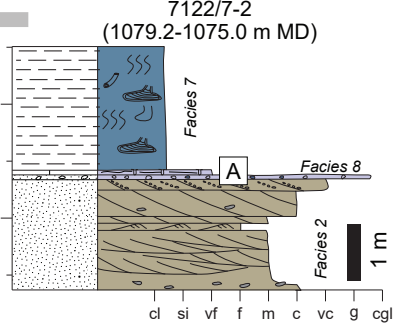
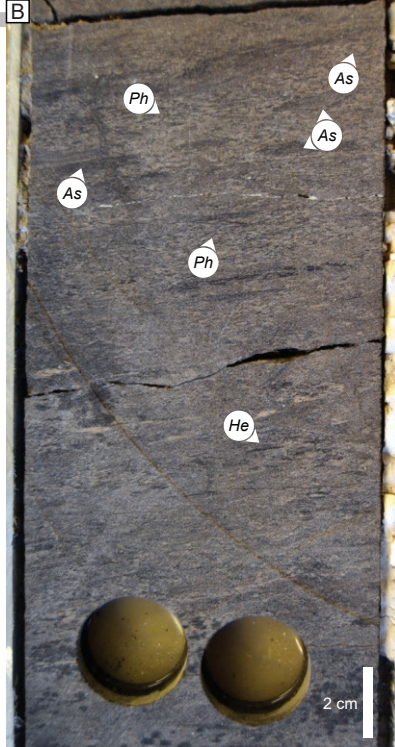
Facies	Interpretation	Lithology	Sedimentary structures and facies architecture	Thickness	BI	Trace fossils and biota	Petrophysical log signatures
1	Distal alluvial fan	Coarse to very coarse-grained sandstone. Poorly sorted. Scattered fine gravel and rare mudstone and siltstone clasts	Sharp-based. Massive (structureless), diffuse low-angle cross-stratification	Bed boundaries indistinct; total thickness 7.5 m	0	None observed	<i>GR</i> : Cylindrical; <i>NP-BD crossplot</i> : Large negative separation (gas effect)
2	Braidplain	Sharp-based, stacked fining upward units. Fine- to very coarse-grained sandstone. Rare silty interbeds and laminae. Poorly to moderately sorted. Rare mudstone rip-up clasts.	Multiple internal scour surfaces. Planar and trough cross-stratification. Rare current ripples in finer-grained intervals	0.1-1.2 m thick beds; stacked 1-5 m thick fining-upward units forming 4.7-10 m thick sandstone bodies	0	Rare coal fragments	<i>GR</i> : Cylindrical; <i>NP-BD crossplot</i> : Small negative separation. Large negative separation where gas-filled
3	Fluvial channels						
	<i>3a Fluvial channels</i>	Sharp-based, fining upward units. Very fine- to very coarse-grained sandstone. Moderately to well-sorted. Mudstone rip-up clasts	Structureless, planar and trough cross-stratification, current ripple lamination, plane-parallel lamination	0.1-1.0 m thick beds; 3-10 m thick fining-upward units	0	Abundant coal fragments and plant material. Locally rooted tops	<i>GR</i> : Cylindrical, bell-shaped, symmetrical; <i>NP-BD crossplot</i> : Weak negative or no separation. Large negative separation where gas-filled
	<i>3b Tide-influenced distributary channels</i>	Very fine- to coarse-grained sandstone. Moderately to well-sorted. Abundant mm-	Sharp-based, fining-upward units. Planar and trough cross-stratification, locally with	0.1-2.0 m thick beds; 1-9 m thick fining-upward	0-2	Undifferentiated vertical sand-filled burrows, and small horizontal burrows.	Similar wireline log signatures as facies 3a

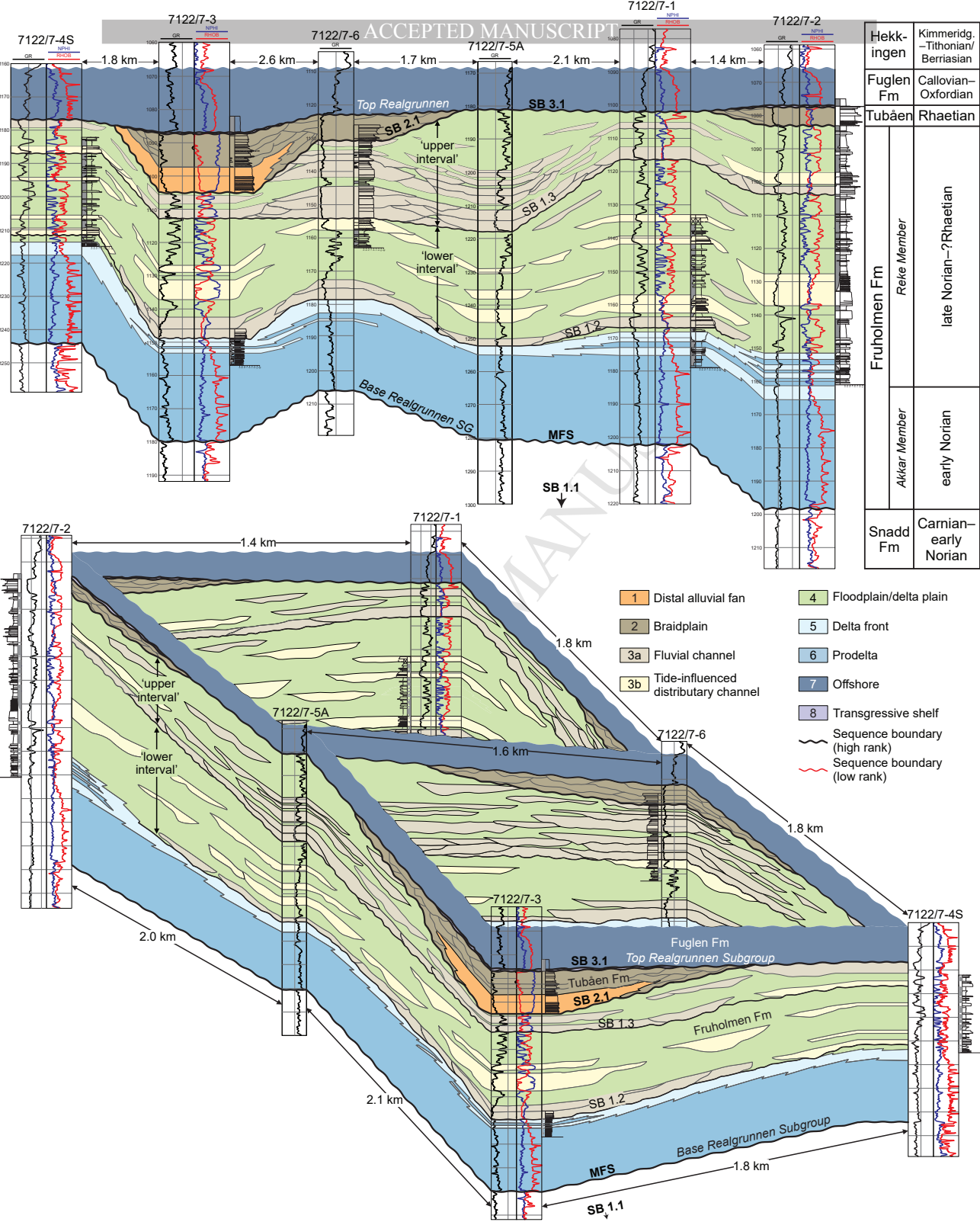
		thick single and paired drapes of mudstone organic debris	tangential set bases, current ripples, flaser lamination, soft-sediment deformation	units		Abundant coal fragments and plant material. Locally rooted tops	
4	Floodplain/delta plain	Grey to brownish grey mudstone, siltstone and very fine- to fine-grained sandstone. Thin coals and carbonaceous mudstone	Mostly massive. Occasional fining and coarsening upward grain-size motifs. Current ripple lamination (2D and 3D ripples, locally climbing), plane-parallel lamination, low-angle planar cross-stratification, rare soft-sediment deformation structures	mm-scale to >1 m thick sandstone beds; total thickness: 1-24 m	0-4	<i>Lockeia</i> , undifferentiated horizontal and vertical burrows. Rootlets, coal fragments and plant material	<i>GR</i> : irregular, serrated; <i>NP-BD crossplot</i> : irregular
5	Delta front	Mainly very fine- to fine grained sandstone. Interbedded grey mudstone and siltstone	Single or stacked coarsening-upward units. Current- and wave-ripple lamination, locally climbing ripples, combined flow ripples, low-angle planar cross-lamination, plane-parallel lamination, dish structures, rare synaeresis cracks	cm-scale to 2.5 m thick sandstone beds in 1-4 m thick coarsening-upward units; total thickness to 5-6 m	1-5	<i>Lockeia</i> , <i>Planolites</i> , <i>Teichichnus</i> , <i>Diplocraterion</i> , <i>Palaeophycus</i> , <i>Rosselia</i> and <i>Skolithos</i> . Rare fugichnia. Impoverished, distal expression of the <i>Skolithos</i> ichnofacies. Rooted tops common. Coal fragments and plant material. Rare shell fragments	<i>GR</i> : locally funnel-shaped, slightly irregular. <i>NP-BD crossplot</i> : weak positive or no separation
6	Prodelta	Grey to dark grey mudstone, interbedded mudstone, siltstone, and	Massive (structureless) to normal-graded beds and laminae. Horizontal lamination, soft-sediment deformation.	mm-scale up dm-thick sandstone beds; total thickness	0-4	<i>Chondrites</i> , <i>Lockeia</i> , <i>Planolites</i> , <i>Rhizocorallium</i> , <i>Rosselia</i> and <i>Teichichnus</i> . Impoverished <i>Cruziana</i>	<i>GR</i> : high response, slightly serrated; <i>NP-BD crossplot</i> : Large positive

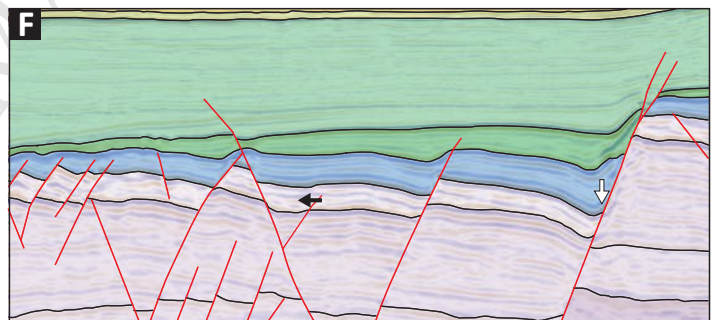
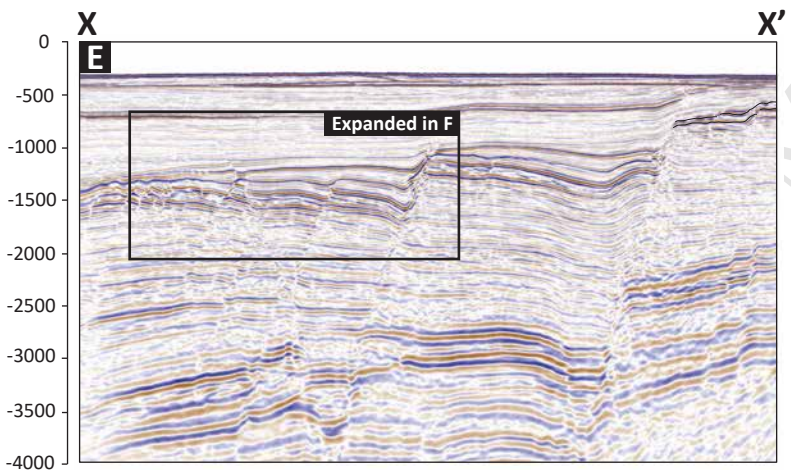
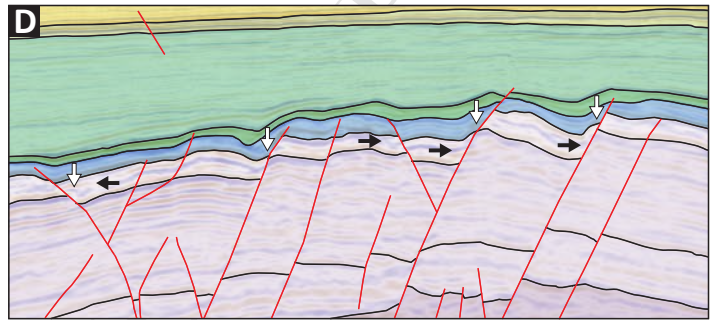
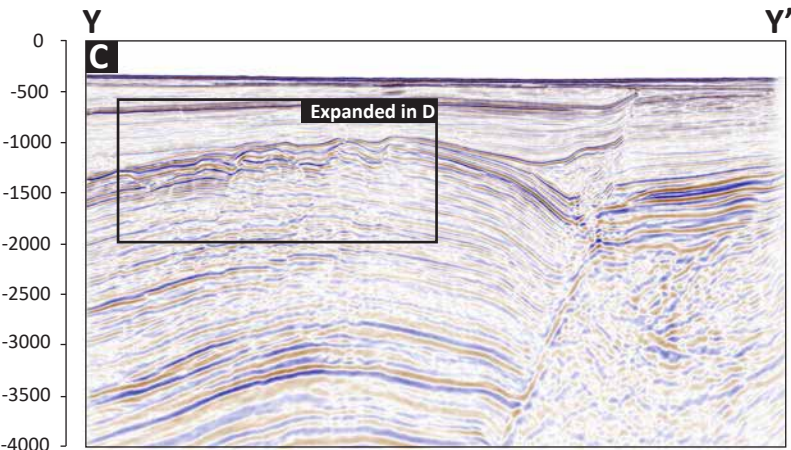
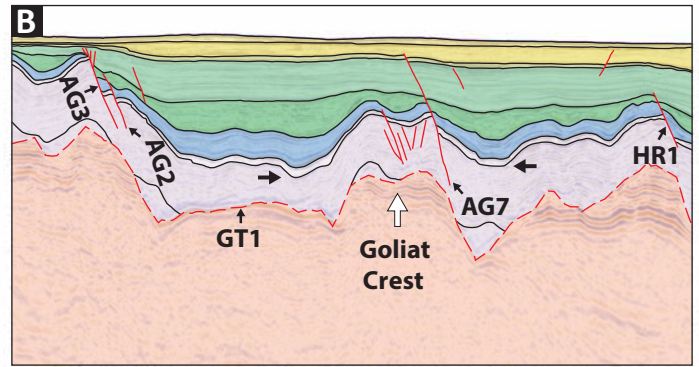
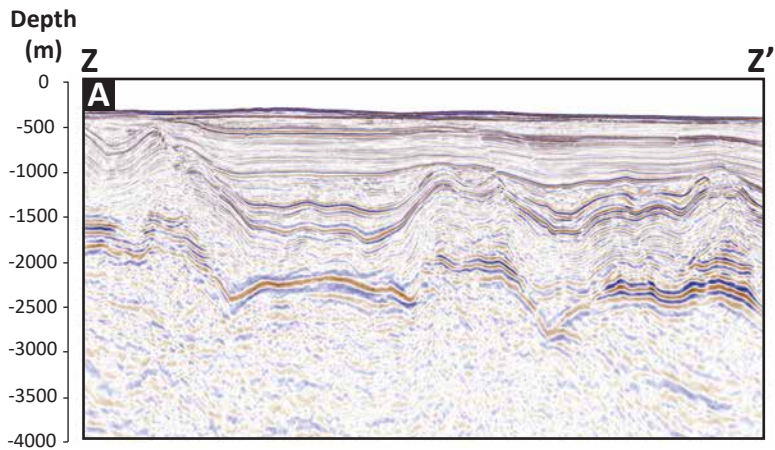
		very fine-grained sandstone	Synaeresis cracks. Wave-, current- and combined-flow ripples observed in sandstone beds	23-33 m including non-cored interval		ichnofacies. Rare shell fragments.	separation, slightly decreasing upward
7	Offshore	Grey, dark grey and brownish grey silty mudstone, and siltstone, locally pyritic	Structureless. Primary sedimentary structures obliterated by bioturbation and/or absent due to lack of lithological contrast	Bed boundaries indistinct; total thickness 10-19 m	4-6	<i>Asterosoma</i> , <i>Chondrites</i> , <i>Helminthopsis</i> , <i>Phycosiphon</i> , <i>Terebellina</i> , <i>Zoophycos</i> . Distal <i>Cruziana</i> ichnofacies. Rare belemnites	GR: high response, serrated; NP-BD crossplot: Relatively large positive separation
8	Transgressive shelf	Polymictic, matrix-supported conglomerate with phosphate and quartz pebbles. Carbonates.	Columnar to irregular lamination in carbonate	15-20 cm	0-3	Sharp-walled, unlined and passively filled vertical burrows attributed to the <i>Trypanites/Glossifungites</i> ichnofacies	No distinct wireline log signatures (below resolution)

Well	Fruholmen Fm, 'lower' interval			Fruholmen Fm, 'upper' interval			Fruholmen Fm, 'lower' and 'upper' intervals combined		
	T _c (m)	T(m)	CDP	T _c (m)	T(m)	CDP	T _c (m)	T(m)	CDP
7122/7-1	13.1	50.5	0.26	5.8	14.4	0.40	64.9	19.1	0.29
7122/7-2	9.6	55.2	0.17	6.5	20.8	0.31	15.1	76	0.20
7122/7-3	14.7	36.3	0.41	5.8	8.1	0.72	20.5	44.3	0.46
7122/7-4S	4.0	24.5	0.16	4.8	10.5	0.46	9.1	35	0.26
7122/7-5A	10.3	34.4	0.30	16.5	36.8	0.45	26.8	71.2	0.38
7122/7-6	10.8	24.5	0.44	19.2	23.6	0.81	29.9	48.1	0.62
Mean			0.29			0.53			0.37

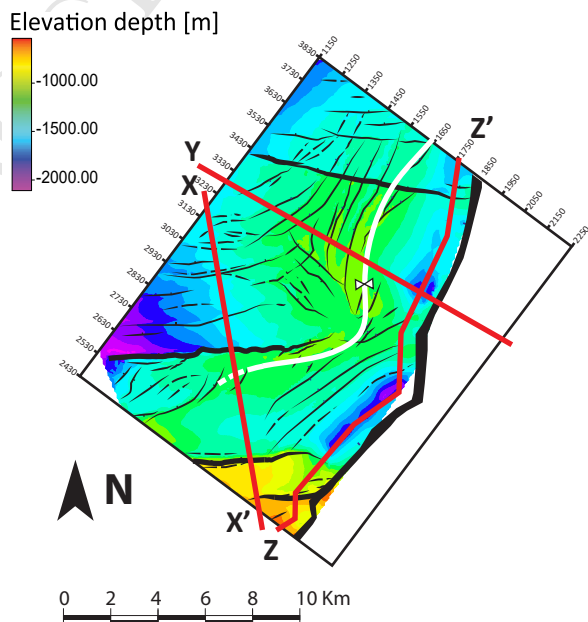
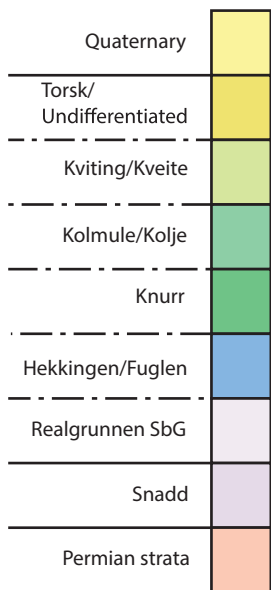




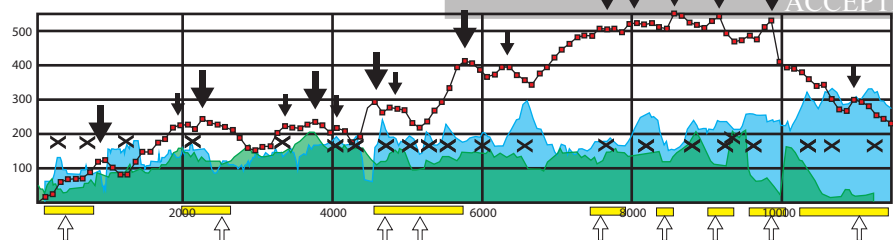




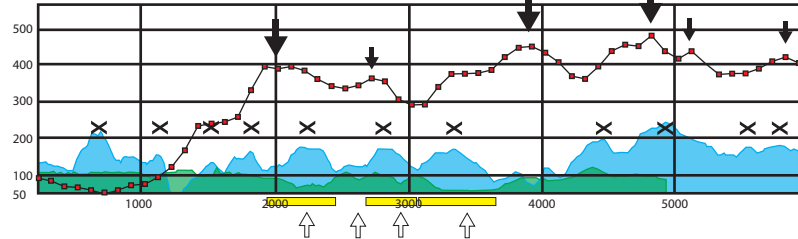
⇩ Up-dragged hanging wall strata
 ← Minor growth wedges



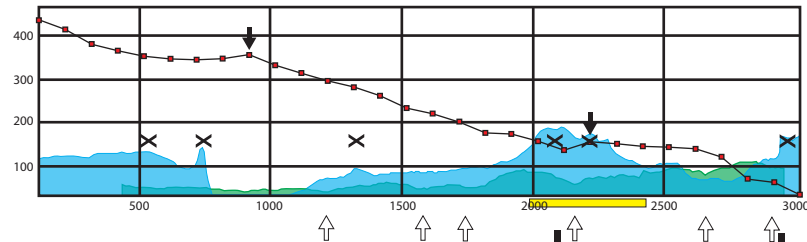
AG1



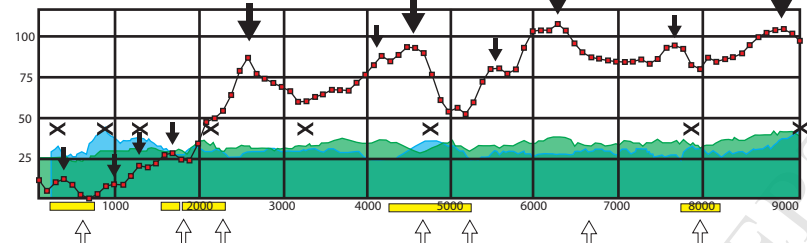
AG2



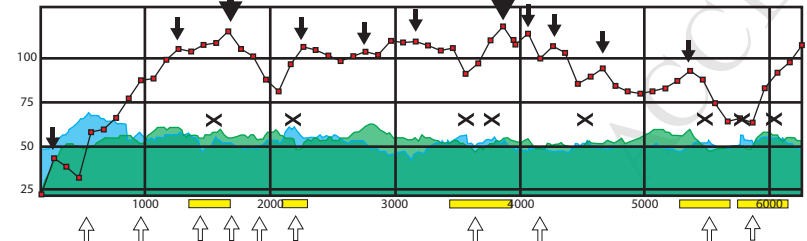
AG3



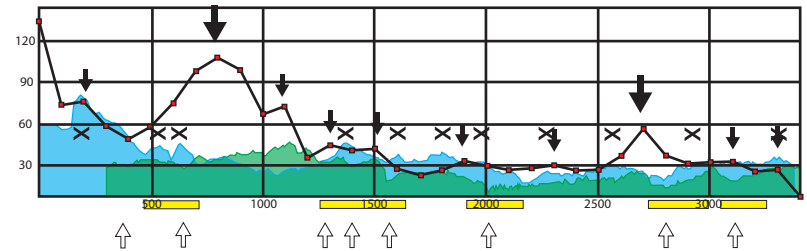
AG5



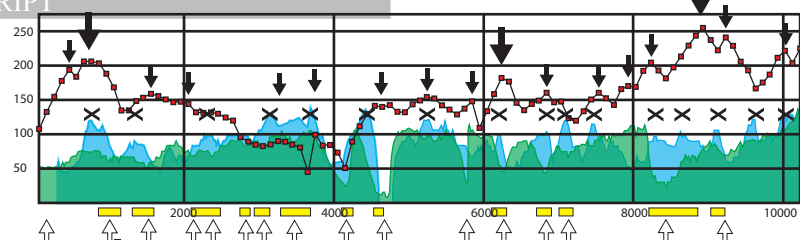
AG6



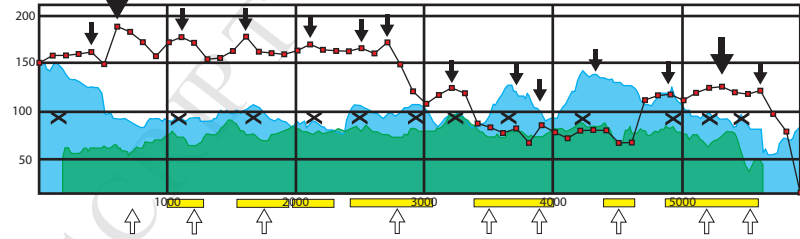
AG7



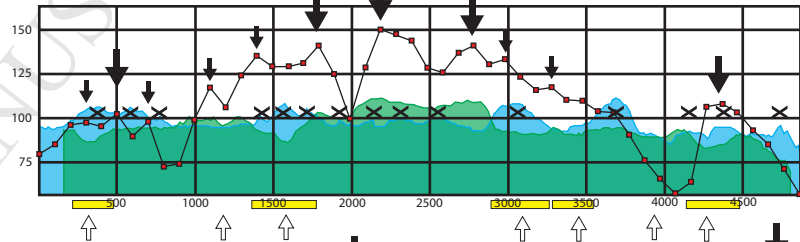
HR1



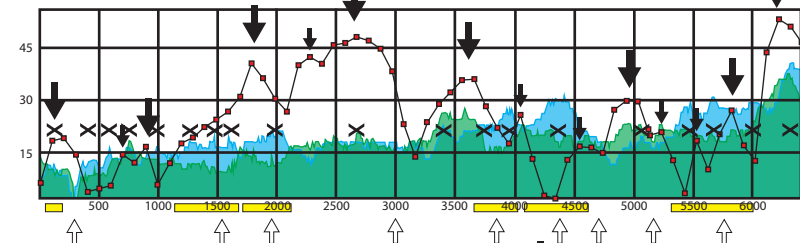
GT2



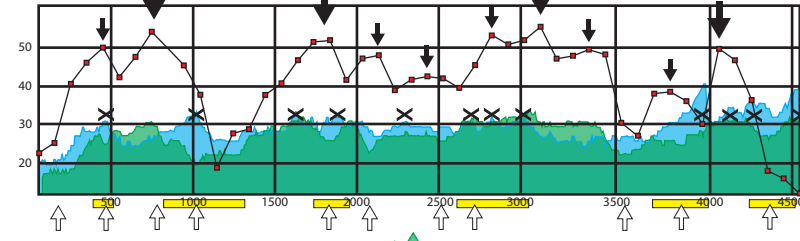
GT3



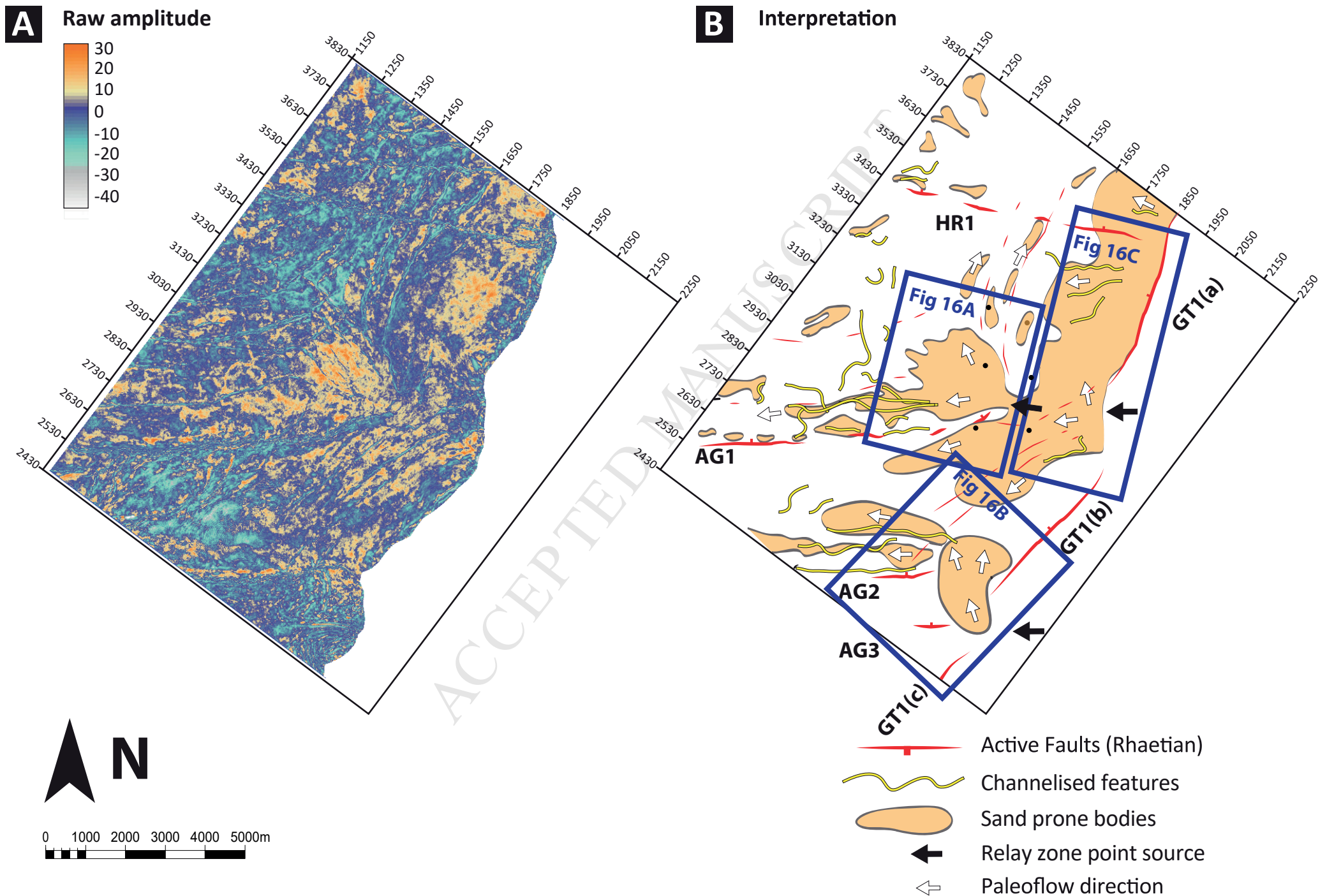
GT4

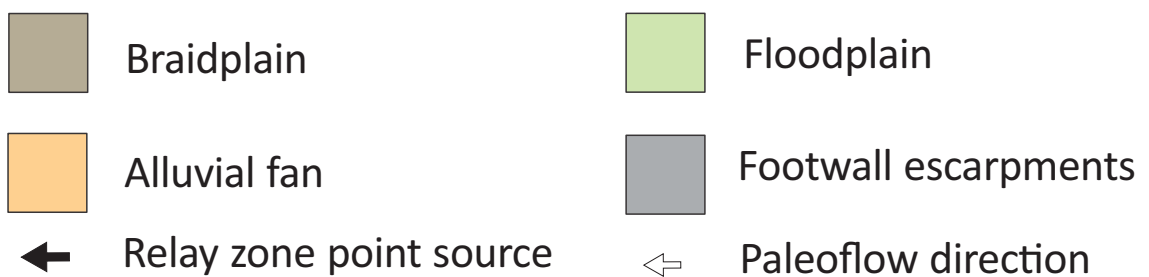
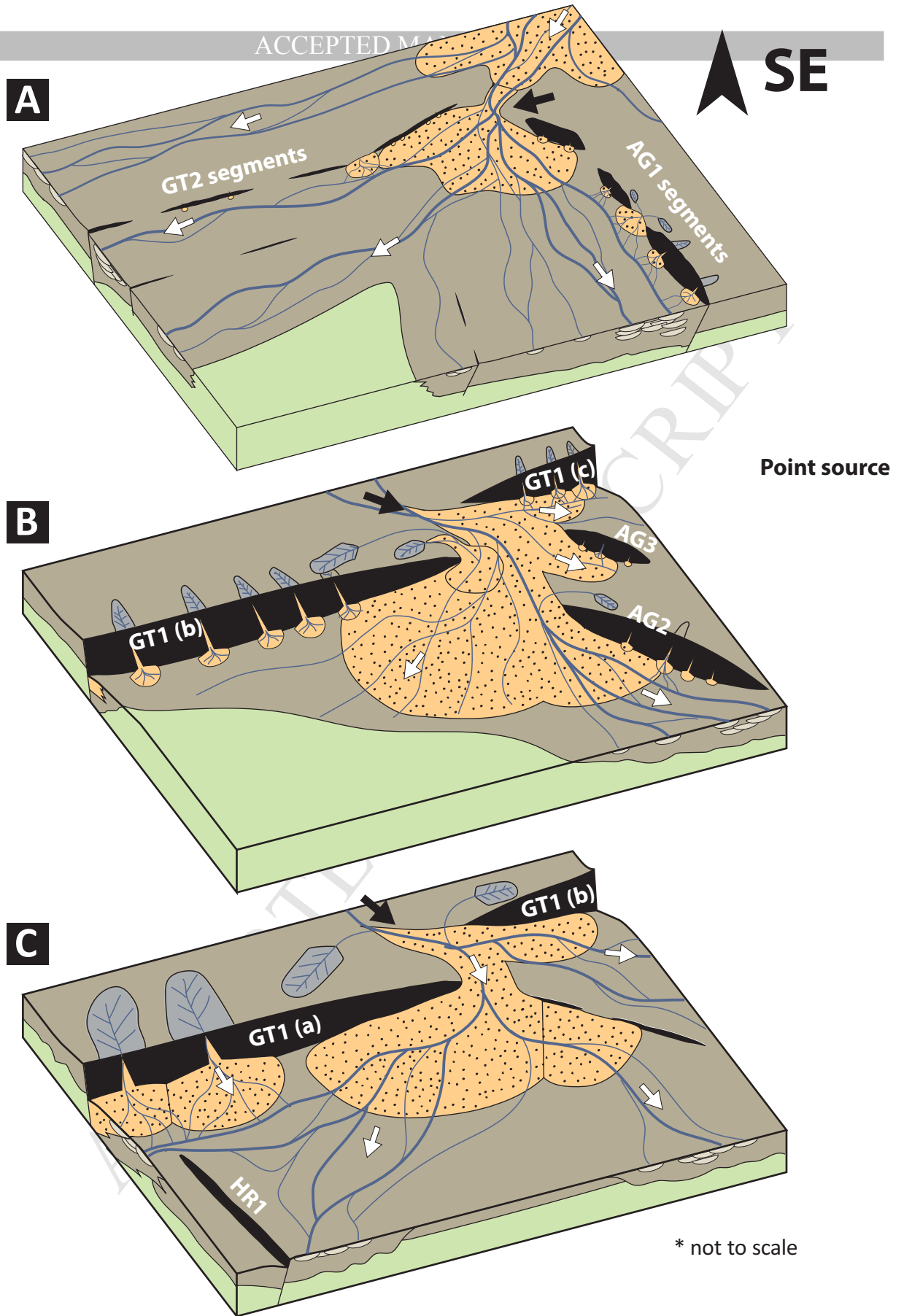


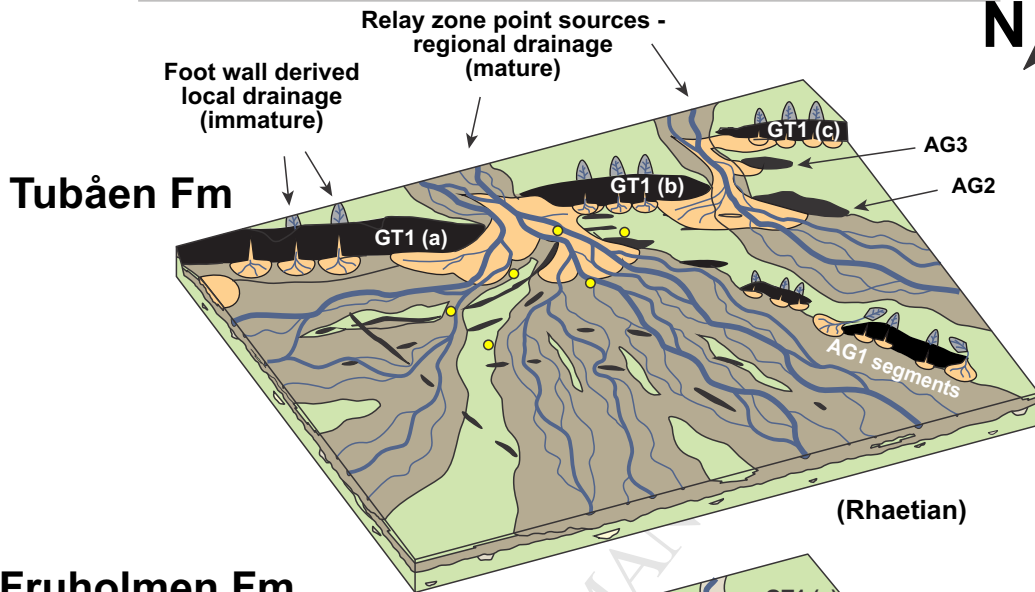
GT5



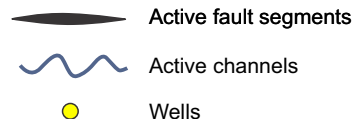
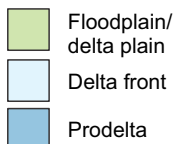
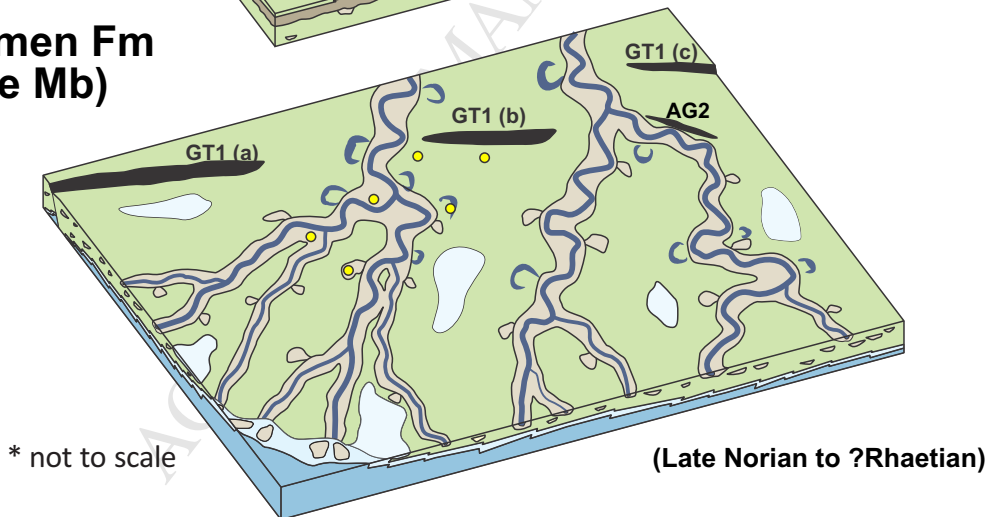
- ↓ Displacement maxima 1st order
- ↓ Displacement maxima 2nd order
- × Hanging wall maxima
- ↑ Footwall minima
- Fault throw profile w/ sample points
- Footwall thickness
- Hanging wall Thickness
- X axis: Fault Trace Distance (m)
- Y axis: Throw/Thickness (m)
- Active Segments

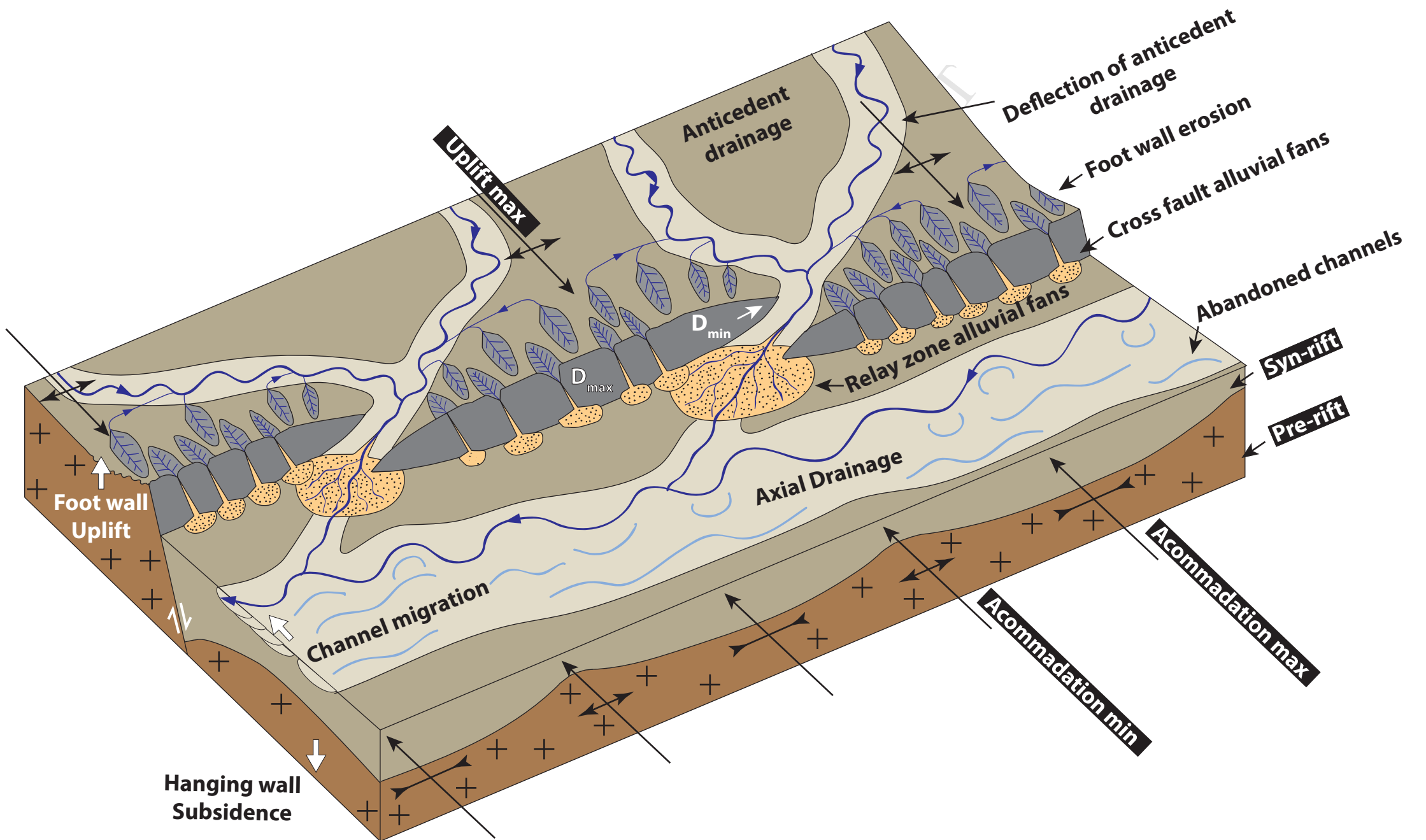


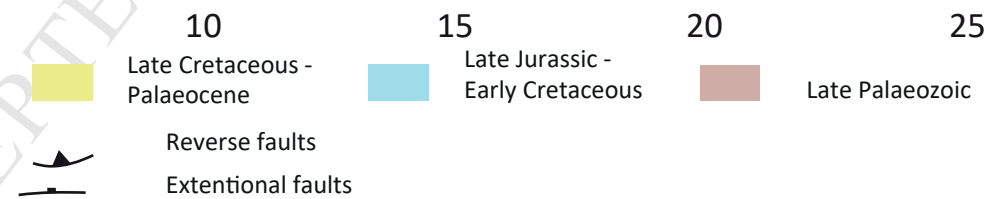
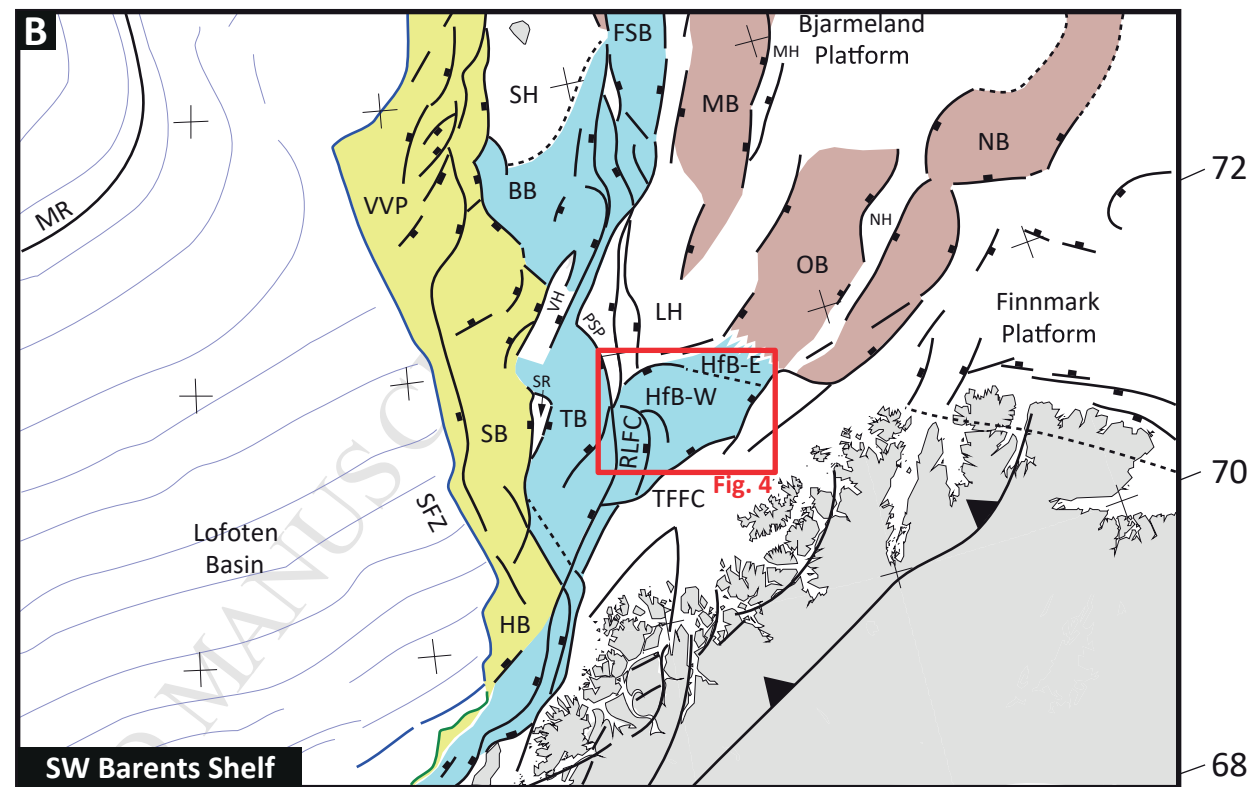
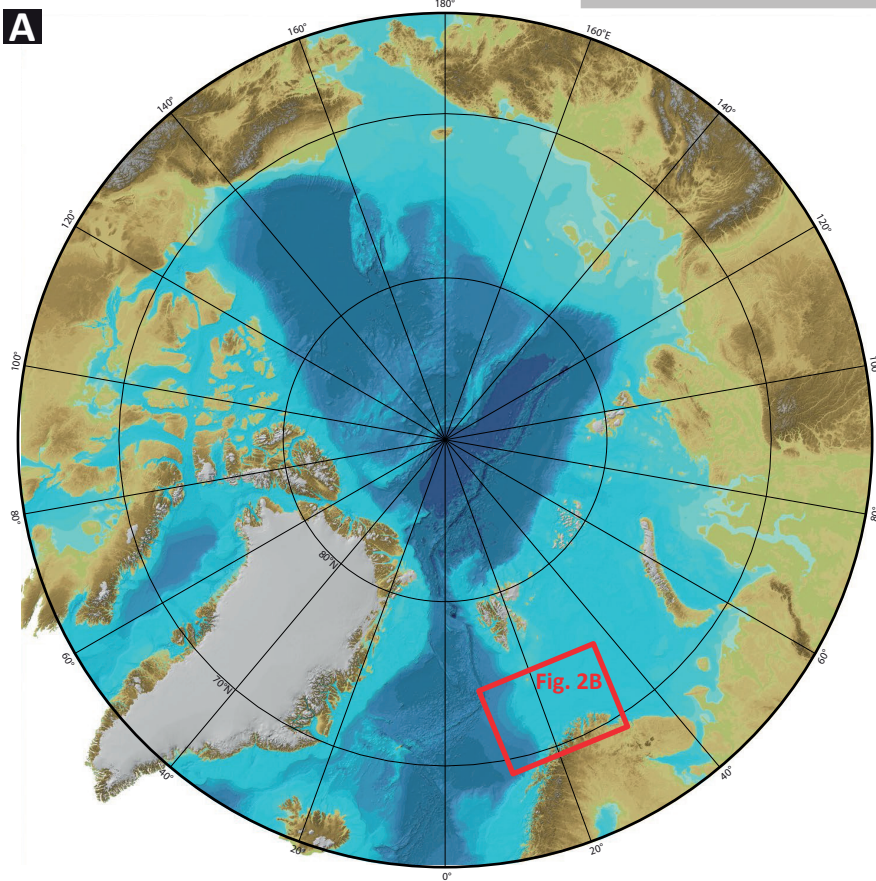




**Fruholmen Fm
(Reke Mb)**



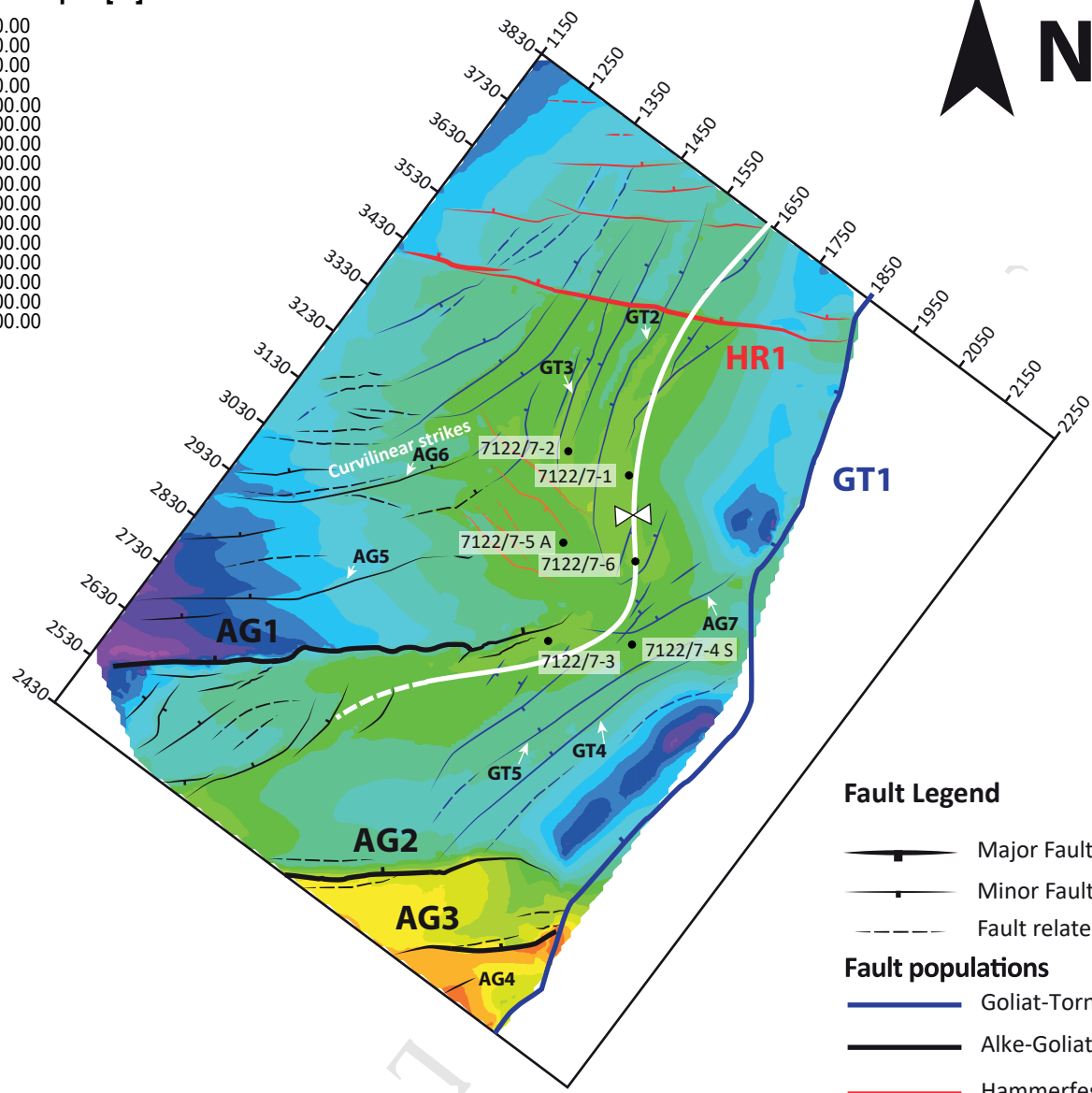
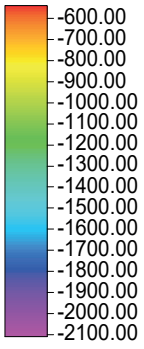




Top Realgrunnen Subgroup surface

ACCEPTED MANUSCRIPT

Elevation depth [m]

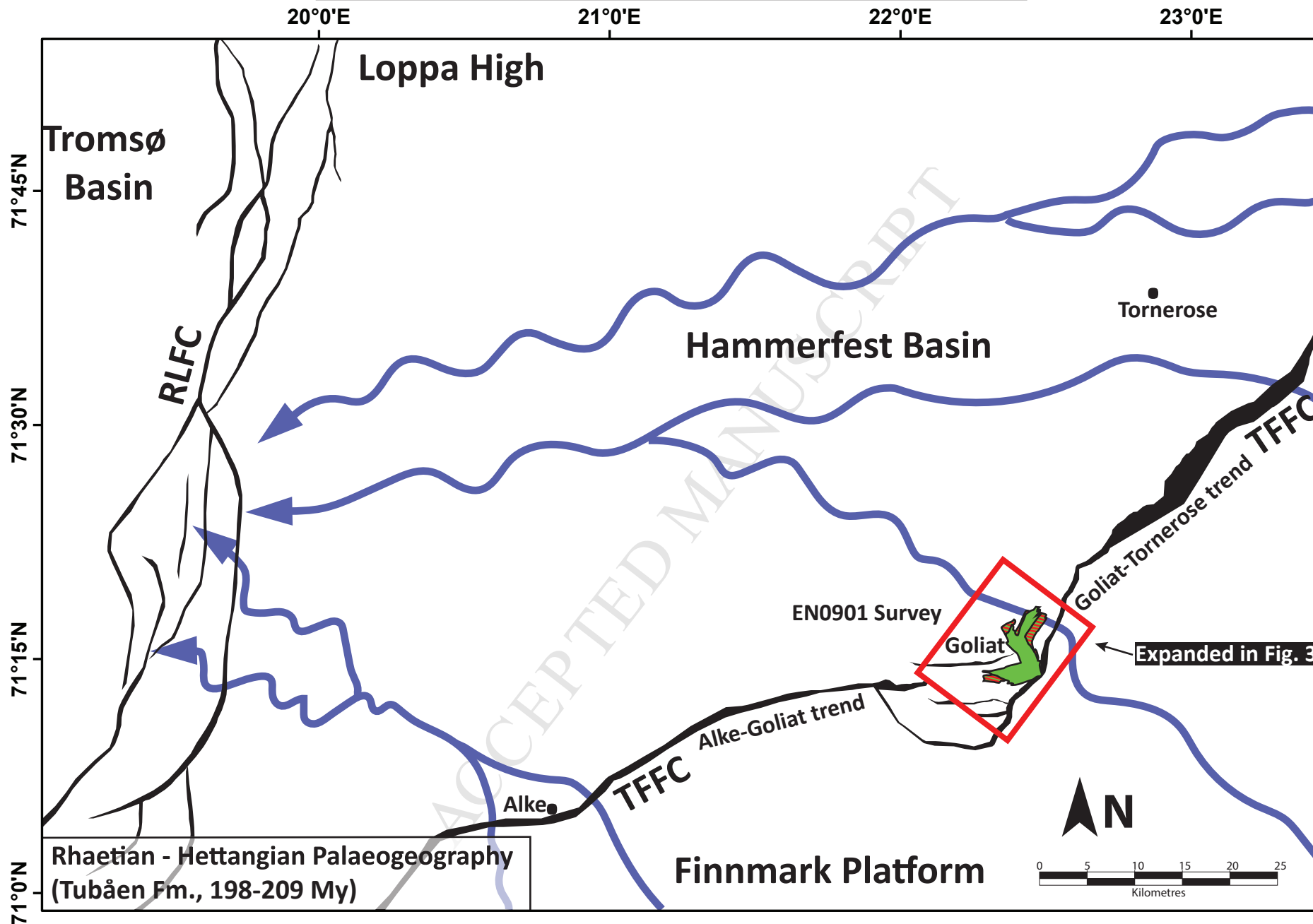




Fault Legend

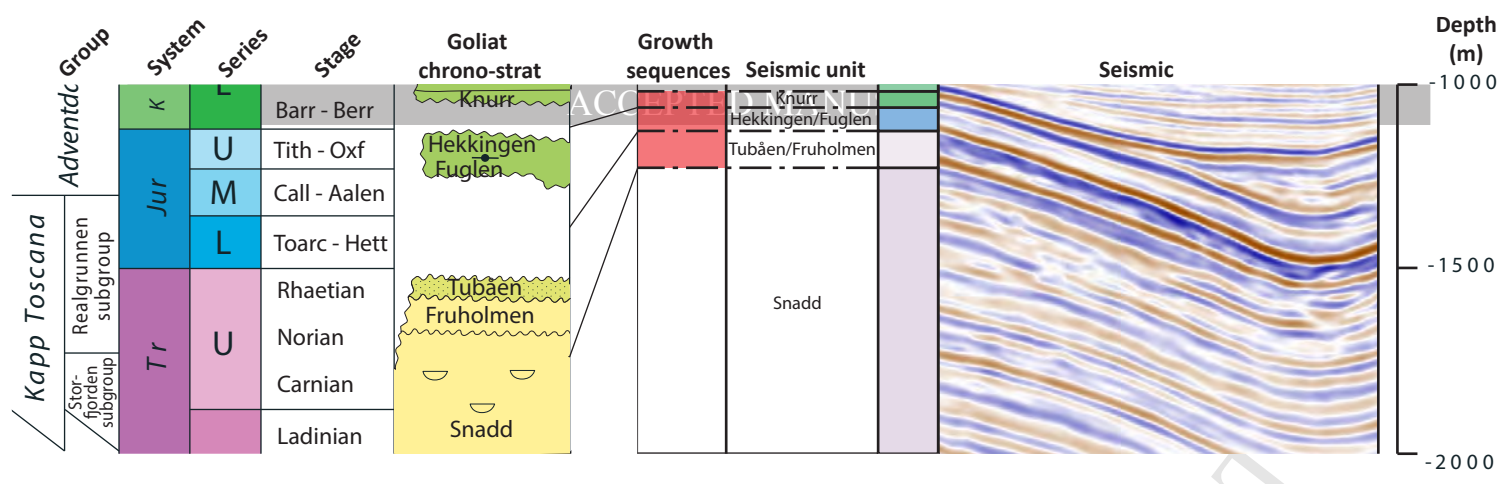
- Major Fault
- Minor Fault
- Fault related Lineament
- Goliat-Tornerose
- Alke-Goliat
- Hammerfest Regional
- Goliat Central
- Fold axial trace



* AG1, 2, 3, 4 and GT1 form segments of the TFFC









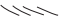
























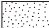





-  Fluvial systems (schematic)
-  Basin delineating faults

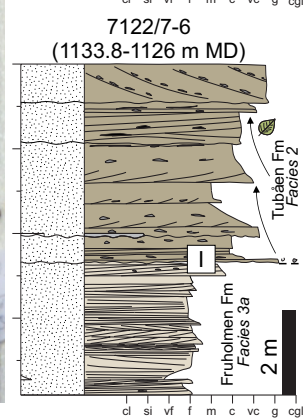
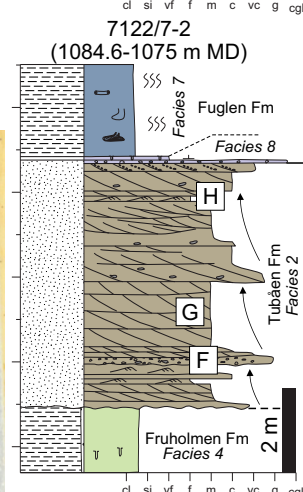
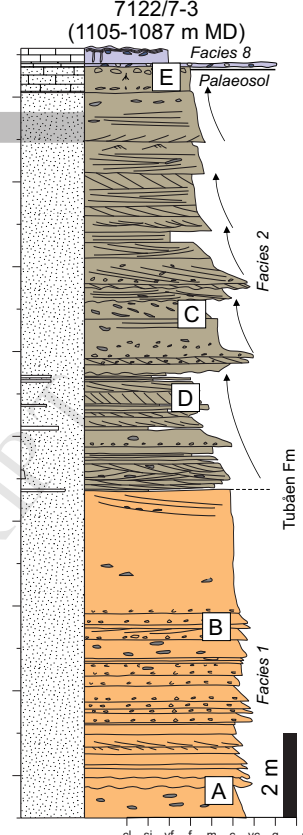
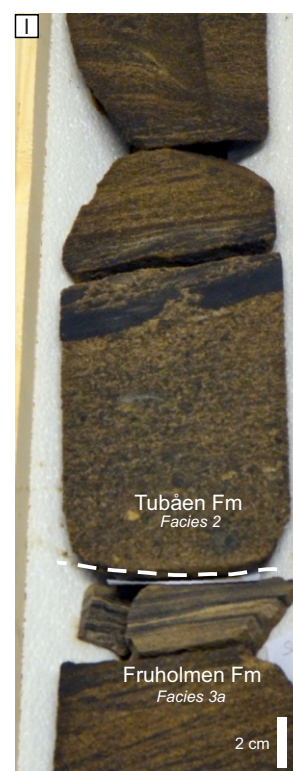
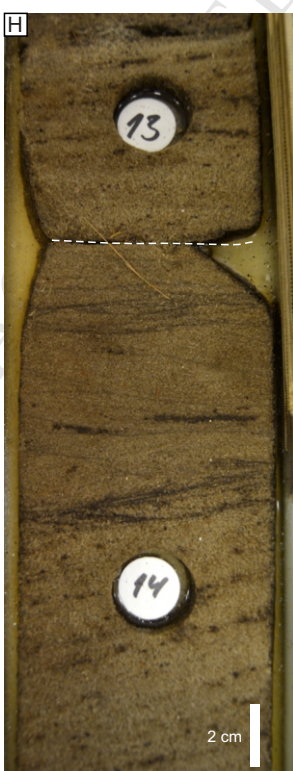


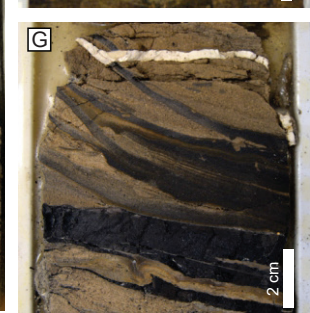
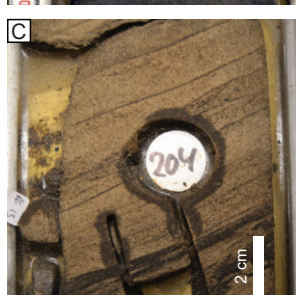
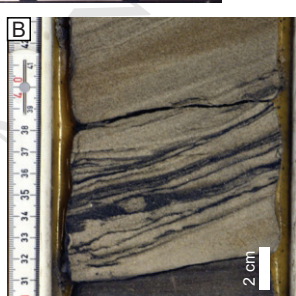
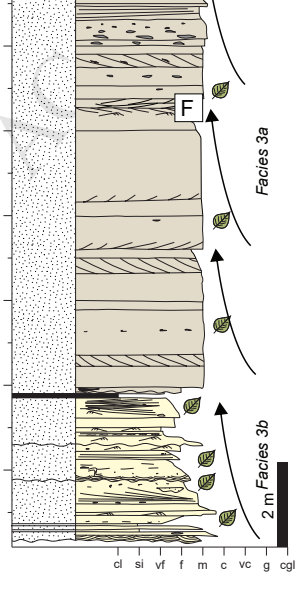
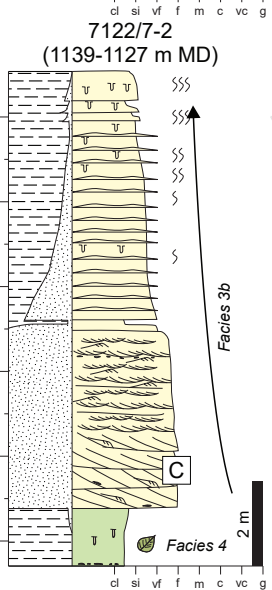
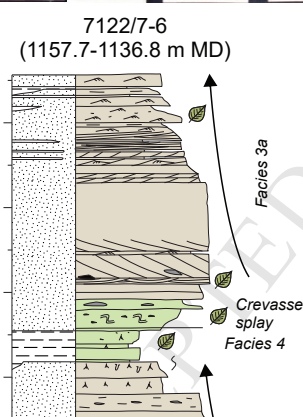
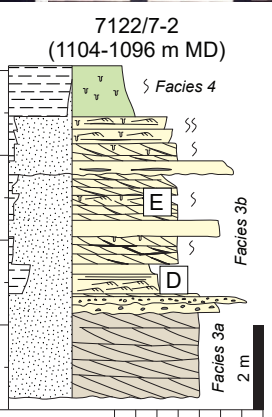
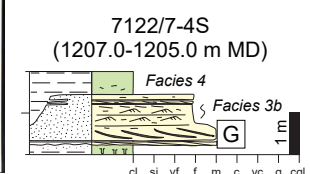
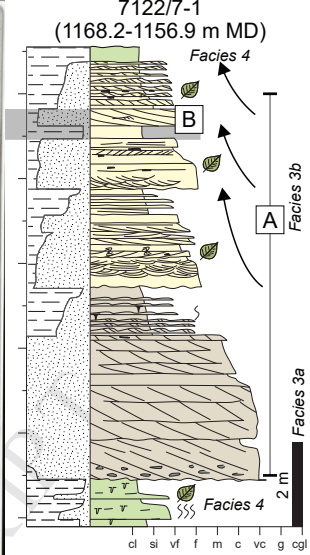
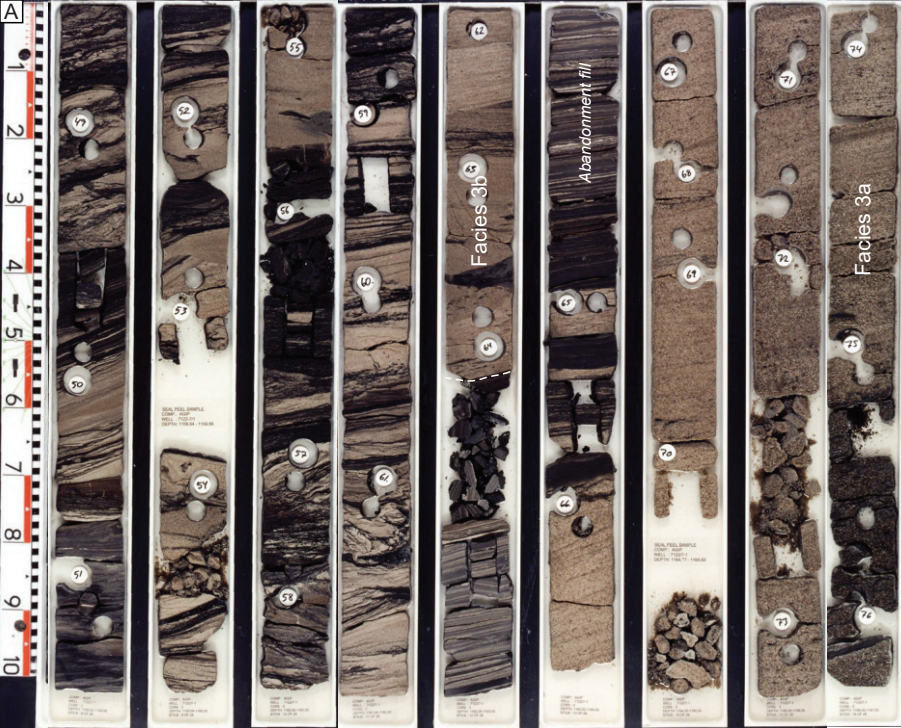
Coastal, deltaic and flood-plain deposits
 Alluvial and fluvial deposits

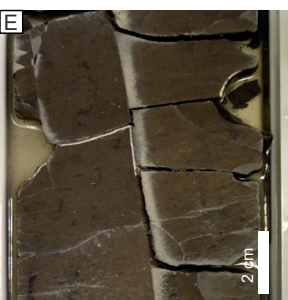
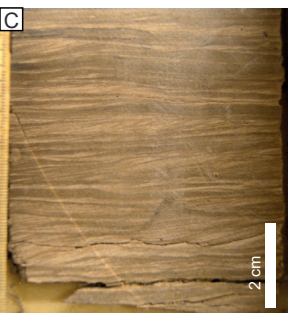
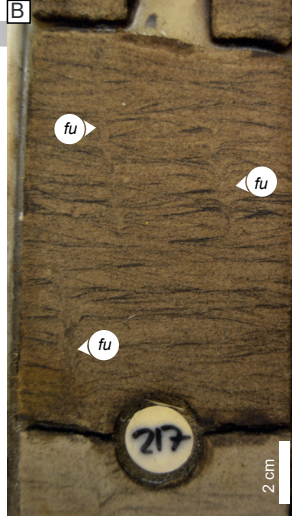
Marine deposits, mainly shale

ACCEPTED MANUSCRIPT

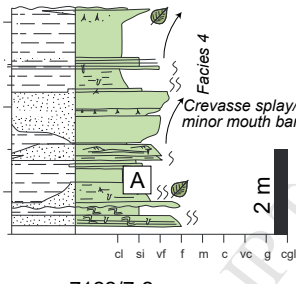
	Calcite cemented		Low-angle cross-stratification		Bioturbation		fugichnia (escape burrow)		<i>Planolites</i>
	Siderite cemented		Planar cross-stratification		Dewatering structure		<i>Asterosoma</i>		<i>Rhizocorallium</i>
P	Phosphorite		Trough cross-stratification		Synaeresis crack		<i>Chondrites</i>		<i>Rosselia</i>
Py	Pyrite		Current ripple		Rootlet/root trace		<i>Diplocraterion</i>		<i>Terebellina</i>
Si	Siderite		Wave ripple		Shell fragment		<i>Lockeia</i>		<i>Teichichnus</i>
	Sharp/erosive or irregular bed contact		Soft-sediment deformation		Belemnite		<i>Helminthopsis</i>		<i>Zoophycos</i>
	Sharp/planar bed contact		Lenticular bedding		Bivalve		<i>Palaeophycus</i>		Sandstone
	Plane parallel lamination/stratification		Flaser bedding		Plant fragment		<i>Phycosiphon</i>		Mudstone



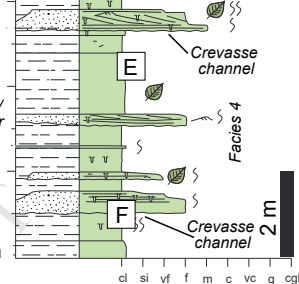




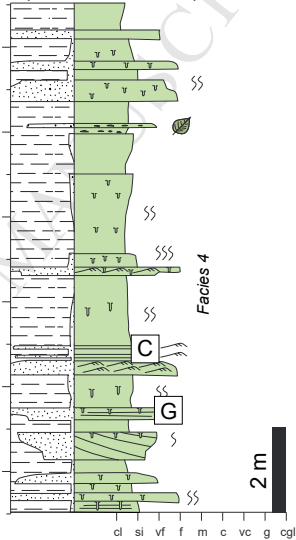
7122/7-6
(1162.8-1157.7 m MD)



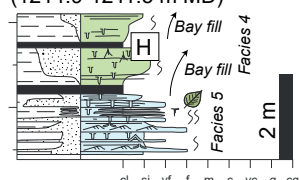
7122/7-4S
(1204-1198 m MD)



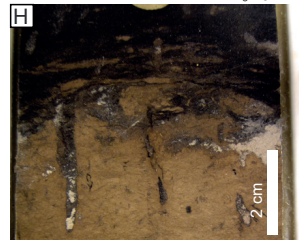
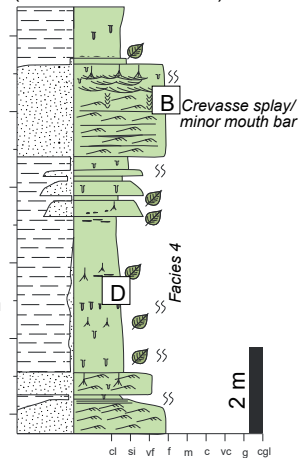
7122/7-2
(1121-1109 m MD)



7122/7-4S
(1214.9-1211.5 m MD)



7122/7-2
(1148.5-1137.2 m MD)



- The Realgrunnen Subgroup contains the upper reservoir interval in the Goliat field located offshore northern Norway.
- We present a sedimentological, fault, and Amplitude versus Angle (AVA) analysis of the Subgroup.
- A minor Norian to Rhaetian tectonic event is recognised affecting the southern Hammerfest Basin during deposition of the Realgrunnen Subgroup.
- Displacement profiles of faults and along-fault thickness variations highlight the early history of fault activity which influenced depositional geometries.
- AVA attribute maps reveal the geometries of gross sand prone depositional bodies, i.e., individual and amalgamated channels, ox-bow lakes and alluvial fans.
- Palaeogeographic reconstructions for the Fruholmen and Tubåen Formations comprising the Realgrunnen Subgroup are presented.